Human pancreatic capillaries and nerve fibers persist in type 1 diabetes despite beta cell loss

Running Title: Innervation and vascularization in type 1 diabetes

Tiffany M. Richardson[1], Diane C. Saunders[2], Rachana Haliyur[1,3], Shristi Shrestha[2,4], Jean-Philippe Cartailler[4], Rachel B. Reinert[5,6], Jenna Petronglo[7], Rita Bottino[8], Radhika Aramandla[2], Amber M. Bradley[2], Regina Jenkins[2], Sharon Phillips[9], Hakmook Kang[9], Human Pancreas Analysis Program[10], Alejandro Caicedo[11,12,13], Alvin C. Powers[1,2,14*], and Marcela Brissova[2*]

[1]Department of Molecular Physiology and Biophysics, Vanderbilt University, Nashville, TN
[2]Department of Medicine, Division of Diabetes, Endocrinology, and Metabolism, Vanderbilt University Medical Center, Nashville, TN
[3]Department of Ophthalmology and Visual Sciences, University of Michigan, Ann Arbor, MI
[4]Creative Data Solutions, Vanderbilt Center for Stem Cell Biology, Nashville, Tennessee, USA
[5]Department of Molecular & Integrative Physiology, University of Michigan Medical School, Ann Arbor, MI
[6]Division of Metabolism, Endocrinology & Diabetes, Department of Internal Medicine, University of Michigan Medical School, Ann Arbor, MI
[7]Department of Pathology, Microbiology, and Immunology, Vanderbilt University Medical Center, Nashville, TN
[8]Imagine Pharma, Pittsburgh, PA
[9]Department of Biostatistics, Vanderbilt University Medical Center, Nashville, TN
[10]Human Pancreas Analysis Program (HPAP; RRID: SCR_016202) of the Human Islet Research Network (RRID: SCR_014393)
[11]Division of Endocrinology, Diabetes, and Metabolism, Department of Medicine, University of Miami Miller School of Medicine, Miami, Florida
[12]Program of Neuroscience, University of Miami Miller School of Medicine, Miami, Florida
[13]Department of Physiology and Biophysics, University of Miami Miller School of Medicine, Miami, Florida
[14]VA Tennessee Valley Healthcare, Nashville, TN

Corresponding authors:

Marcela Brissova
Vanderbilt University Medical Center
7465 Medical Research Bldg IV
2213 Garland Avenue
Nashville, TN 37232-0475
E: marcela.brissova@vanderbilt.edu
T: (615) 936-1729

Alvin C. Powers
Vanderbilt University Medical Center
7465 Medical Research Bldg IV
2213 Garland Avenue
Nashville, TN 37232-0475
E: al.powers@vumc.org
T: (615) 936-7678

ABSTRACT

The autonomic nervous system regulates pancreatic function. Islet capillaries are essential for the extension of axonal projections into islets, and both of these structures are important for appropriate islet hormone secretion. Because beta cells provide important paracrine cues for islet glucagon secretion and neurovascular development, we postulated that beta cell loss in type 1 diabetes (T1D) would lead to a decline in intra-islet capillaries and reduction of islet innervation, possibly contributing to abnormal glucagon secretion. To define morphological characteristics of capillaries and nerve fibers in islets and acinar tissue compartments, we analyzed neurovascular assembly across the largest cohort of T1D and normal individuals studied thus far. Because innervation has been studied extensively in rodent models of T1D, we also compared the neurovascular architecture between mouse and human pancreas and assembled transcriptomic profiles of molecules guiding islet angiogenesis and neuronal development. We found striking inter-species differences in islet neurovascular assembly but relatively modest differences at transcriptome level, suggesting post-transcriptional regulation may be involved in this process. To determine if islet neurovascular arrangement is altered following beta cell loss in T1D, we compared pancreatic tissues from non-diabetic, recent-onset T1D (<10 years duration), and longstanding T1D donors (>10 years duration). Both islets and acinar tissue had greater capillary density in recent-onset T1D accompanied by overall greater islet nerve fiber density in recent-onset and longstanding T1D as visualized by a pan-neuronal marker. We did not detect changes in sympathetic axons in either T1D cohort. Additionally, nerve fibers overlapped with extracellular matrix (ECM), supporting its role in the formation and function of axonal processes. These results indicate that pancreatic capillaries and nerve fibers persist in T1D despite beta cell loss, suggesting that alpha cell secretory changes may be decoupled from neurovascular components.

NEW & NOTEWORTHY

Defining the neurovascular architecture in the pancreas of individuals with T1D is crucial to understanding the mechanisms of dysregulated glucagon secretion. In the largest T1D cohort of biobanked tissues analyzed to date, we found that pancreatic capillaries and nerve fibers persist in human T1D despite beta cell loss, suggesting that alpha cell secretory changes may be decoupled from neurovascular components. Because innervation has been studied extensively in rodent T1D models, our studies also provide the first rigorous direct comparisons of neurovascular assembly in mouse and human indicating dramatic inter-species differences.

INTRODUCTION

Hormone secretion from pancreatic islets of Langerhans is essential to maintain blood glucose levels within a narrow physiological range. Vascular and neuronal inputs to the islet aid in the regulation of coordinated hormone secretion (1–5). Alpha cells within the islet secrete glucagon to counterbalance insulin secretion by beta cells and prevent hypoglycemia. In type 1 diabetes (T1D), alpha cell function is dysregulated with loss of glucagon secretion in response to hypoglycemia (6, 7), which interestingly precedes a secretory impairment of major alpha cell stimulus, epinephrine, produced by adrenal chromaffin cells (7). Paradoxically, individuals with T1D secrete more glucagon during mixed-meal stimulation (8, 9). Recurrent hypoglycemic episodes, which correlate with progressive beta cell loss in T1D, lead to an impairment of sympathoadrenal responses and the risk of a life-threatening hypoglycemia unawareness syndrome, also known as hypoglycemia-associated autonomic failure (10). Additionally, autonomic dysfunction could be further exacerbated with disease duration, and progressive diabetic neuropathy may affect autonomic innervation of the pancreatic islet (1, 7, 8, 11). Thus, defining the neurovascular architecture in the pancreas of individuals with T1D is crucial to understanding the mechanisms of dysregulated glucagon secretion.

Studies from rodent and human T1D pancreatic tissues provide a spectrum of inferences on disease-associated intra-islet innervation phenotypes. Work first done in rodent models of T1D, such as the BioBreeder (BB) rat and nonobese diabetic (NOD) mouse, showed a loss of intra-islet sympathetic nerve fibers associated with insulitis and decreased glucagon secretion in response to tyramine-mediated norepinephrine release (12–16). By contrast, a recent study used optically cleared tissue from NOD mice to show an increase in islet nerve fibers (17). Other studies, however, revealed considerable inter-species differences in intra-islet nerve fiber and capillary densities, thus raising concerns about whether the data from rodent models reflect the findings about human islet neurovascular architecture in T1D (18–21). Moreover, two recent

studies of human pancreatic sympathetic innervation in short-duration T1D reached opposing conclusions as well; one study indicated an early decline in islet sympathetic nerve density in T1D (22), while the other one showed no significant differences between non-diabetic and short-duration T1D donor islets (23). Interestingly, the latter study found that pancreata from autoantibody-positive (AAb+) human donors had lower sympathetic nerve fiber density, specifically within pancreatic islets (23). In addition, Lundberg et al. showed that the second arm of the autonomic nervous system, parasympathetic nerve fibers, may also be altered in human T1D (24). Considering the developmental and functional links between vascularization and innervation (25–27), it is noteworthy that islet vessel density was found to be greater in short-duration T1D than in non-diabetic donors (28).

Thus, there is a need to systematically define changes in the human neurovascular architecture across a broader range of T1D duration and large cohort, including not only islet but also acinar tissue compartment, since both appear to be influenced in the disease process (29, 30). Because innervation has been studied extensively in rodent T1D models, we first compared the islet neurovascular architecture between mouse and human. We found dramatic inter-species differences that were not easily explained by transcriptomic profiles of factors guiding angiogenesis and neuronal development. Next, we performed high throughput morphometric analyses of the islet neurovascular architecture in thin human pancreatic tissue sections from a large cohort of bio-banked tissues, including 15 recent-onset and 12 longstanding T1D donors, and compared them to 11 non-diabetic controls. We found that islets and acinar tissue had greater capillary density in recent-onset T1D. This was accompanied by overall increases in islet nerve fiber densities visualized by a pan-neuronal marker in both early-onset and longstanding T1D. We did not detect changes in sympathetic axon densities in T1D tissues. Further assessment of 3D reconstructions from thicker sections (30 μm versus 10 μm) highlighted the persistence of intra-islet nerves in T1D donors and a relationship between

pancreatic nerves, blood vessels, and extracellular matrix (ECM). Collectively, our data indicate that islet capillaries and nerve fibers persist in T1D, suggesting that alpha cell secretory changes may be decoupled from neurovascular components.

RESEARCH DESIGN AND METHODS

Mice

Animal studies were approved by the Institutional Animal Care and Use Committee at Vanderbilt University Medical Center, and animals were kept in facilities monitored by the Vanderbilt University Division of Animal Care. Pancreata from anesthetized C57BL/6 wildtype mouse (N = 10; adult males > 10 weeks old) were collected, lightly paraformaldehyde (PFA)-fixed in 4% PFA in 1X PBS, cryoprotected in 30% w/w sucrose, and frozen in Tissue-Tek Optimal Cutting Temperature (OCT) compound before cryosectioning (26).

Human subjects

Pancreata from non-diabetic (N = 11) and T1D (N = 27) donors were obtained through partnerships with the International Institute for Advancement of Medicine (IIAM), National Disease Research Interchange (NDRI), the Human Pancras Analysis Program (HPAP), and local organ procurement organizations. Pancreata were processed in Pittsburgh by Dr. Rita Bottino or at the University of Pennsylvania through the HPAP T1D program for both islet isolation and histological analysis, as previously described (31, 32). Donor information is detailed in **Table 1** and **Supplemental Table 1**. De-identified medical records provided information for T1D staging. The Vanderbilt University Institutional Review Board declared that studies on de-identified human pancreatic specimens do not qualify as human subject research.

Human procurement and immunohistochemical analysis

Pancreata from non-diabetic and T1D donors (see **Table 1** and **Supplemental Table 1** for donor information) were received within 18 hours from cross-clamp, maintained in cold preservation solution on ice, and processed as described previously (31, 32). Importantly, fixation methodologies were similar between mouse and human pancreatic tissue. Multiple 10 µm and 30 µm serial cryosections from the pancreatic head, body, and tail regions of 27 T1D

and 11 age-matched non-diabetic donors were lightly PFA-postfixed in 1% PFA in 1X PBA and then labeled for immunofluorescence as described previously (31, 32). Primary and secondary antibodies and their working dilutions are listed in **Supplemental Table 2** and **3**. Acinar tissue was visualized by DAPI nuclear counterstain, and islet location was defined by hormone markers. Insulin and glucagon labeling was visualized on the same fluorescence channel unless otherwise indicated due to a maximum of 4 imaging channels available per section for this immunofluorescence paradigm.

Morphometric analysis of 2-D images

Digital images of 10 µm cryosections were acquired with a ScanScope FL (Aperio) for human tissue and a Leica DMI6000 B Microscope (Leica Biosystems) for mouse tissue. These images were then analyzed using MetaMorph v 7.10 software (Molecular Devices LLC). Analyses were run on manually annotated islets (region of interest, ROI) identified by hormone staining. Three equally sized ROIs, outside of islet annotations, were randomly selected per image for acinar measurements. Large nerve fiber bundles and vessels around pancreatic ducts and ganglia were excluded from formal analyses. Intensity thresholding was set per image per individual fluorescence channel to collect object data using the Integrated Morphometry Analysis function (MetaMorph).

For innervation measurements, a pixel filter was set to ≥ 0.463 µm to avoid the inclusion of single pixels as neural fibers. A pixel filter was set to ≥ 2.000 µm for vasculature analysis to prevent the inclusion of single pixels and non-vascular structures while also accounting for average islet vessel diameters determined by previous studies to be between 2-10 µm (20, 28, 33). Islet and acinar nerve fiber length, nerve fiber density, and vascular density were calculated by dividing MetaMorph output by the total ROI area. The analyzed islet area was similar between groups (**Supplemental Fig. 11**). We analyzed an average of 34 ± 1 islets with cross-sectional diameter >50 µm / donor / condition. For a donor to be included in aggregate

analyses, a minimum of 10 islets needed to be assessed. Detailed metrics can be found in respective figure legends.

Analysis of ECM overlap with nerve fibers

Digital images of 30 µm sections were acquired with Zeiss LSM880 (Zeiss Microscopy Ltd) or Olympus FV3000 (Olympus) microscopes. Z-stacks were assembled to generate 3D reconstructions and max intensity projections with cellSens (Olympus) and ZEN (Zeiss) software. To quantify the overlap between the pan-neuronal marker (TUBB3) and ECM marker (COLIV), we used Mander's coefficients generated from the ImageJ plugin "Just Another Co-localization Plugin" (https://imagej.nih.gov/ij/plugins/track/jacop2.html).

Image processing

All confocal images underwent deconvolution and were then displayed as maximum intensity projections. Nearest neighbor-constrained iterative algorithms were employed with the cellSens v3.1 (Olympus). Z-Stack and 3D reconstruction videos were made using cellSens, Imaris v9.8 (Oxford Instruments), or ImageJ software and exported as mp4 files.

Mouse versus human transcriptomic profile comparison

Previously published data was queried to determine general expression profiles of angiogenic, neuronal, and morphogenic pathways and extracellular matrix components in mouse and human islet cells. Gene lists were compiled by authors based on previous publications *(25, 34)* and HGNC-curated gene group pages *(35)*. Normalized count matrices were accessed from bulk RNA-seq datasets as follows: mouse beta and endothelial cells, GSE163825 *(34)*; human endothelial cells, GSE157546 *(36)*; human beta cells, *(37)*. Raw single-cell (sc) datasets were accessed as follows: mouse, GSE159844 *(38)*; human, GSE183568 *(39)*. See **Supplemental Table 4** for information on experimental parameters, sample sizes, and specific samples utilized. For sc mouse dataset, wildtype samples were processed and visualized by uniform

manifold alignment projection (UMAP) using 30 PCA dimensions, and KNN-based clustering was performed with a resolution of 0.5 in Seurat *(40)* yielding 18 clusters. A total of 6 clusters were removed based on strong expression of exocrine markers or mixed cell type assignment, then further clustering of remaining cells (30 dimensions at resolution = 1) yielded 21 clusters. Cell-type assignment was determined using canonical markers (see **Supplemental Table 4**) for endocrine, endothelial, and immune cell populations, and multiple clusters expressing the same canonical markers were combined as applicable. Stellate cells could not be resolved from endothelial cells in this dataset. For sc human dataset, clustering was performed as previously described *(39)*, with technical replicates combined and donor values averaged. In **Fig. 1g-h**, **2g**, and **Supplemental Fig. 5**, for clarity, only genes expressed in >2% of cells in cell types were kept (sc), and log2 expression >8 (bulk) were graphed. All values will be provided in a data file upon publication.

Statistical analysis

Statistical tests are described in the figure legends and text where appropriate. Data are represented as mean ± standard error (SEM), with each mouse or donor considered as N = 1. Outliers were determined and excluded from analyses using the Robust regression and Outlier removal (ROUT) method with Q = 1%. P-values < 0.05 were considered significant and non-significant p-values are designated with “ns” or not denoted. Statistical comparisons were performed using GraphPad Prism software 8.0-9.3 and R version 4.1.2.

Data and Resource Availability

The raw datasets analyzed in this study are already available or will be provided to the journal upon publication (**Supplemental Table 5**). Processed Seurat-object data will be available from corresponding authors upon request and placed into a publicly available database.

RESULTS

Neurovascular architecture of pancreatic islets and acinar tissue differs significantly between mouse and human. To better understand prior reports of inter-species differences in neurovascular architecture, we first defined the neurovascular architecture in non-diabetic mouse pancreas, focusing on both islets and acinar tissue, and compared it to human. Blood vessels were visualized by immunofluorescence labeling for platelet endothelial cell adhesion molecule 1 (PECAM-1), nerve fibers were labeled for pan-neuronal marker tubulin beta 3 (TUBB3), and islet beta and alpha cells were co-labeled for insulin (INS) and glucagon (GCG), respectively. To confirm TUBB3 immunolabeling of nerve fibers in human tissue, we assessed 30 laser-scanning confocal microscopy images where individual image tiles (captured at 10x magnification) were stitched to visualize the entire pancreatic tissue sections. Additionally, we reviewed over 1,000 whole-slide images (captured at 20x magnification) that were used for our high-throughput morphometric analyses. We found many TUBB3+ inter-lobular nerve fiber bundles throughout our tissues demonstrating the utility of this neuronal marker (**Supplemental Fig. 1**). We then utilized morphometric analyses to measure capillary and nerve fiber structural characteristics (**Supplemental Fig. 2a-c**). Using this approach, we found striking inter-species differences; capillaries were much more abundant in mouse islets compared to human (**Fig. 1a-b**), with capillary density being greater in islets than acinar tissue in both species (**Supplemental Fig. 3a-b**). The capillary size was similar in the islet and acinar tissue compartments in mouse and human (**Fig. 1e-f, Supplemental Fig. 3c-d**).

To investigate possible explanations for the species differences in vascularization with emerging islet bulk and single-cell RNA-sequencing data, we compared the transcriptional profile of angiogenic factors and their cognate receptors in cells from mouse and human islets using existing resources and, for the first time in this context comprehensively assessed mouse and human islet datasets side-by-side. The cell-specific expression of angiogenic ligand and

receptor transcripts was similar in bulk, and single-cell (sc) RNA-sequencing (RNA-seq) datasets from mouse (34, 38) and human (36, 37, 39) islets (**Fig. 1g**), notably with high VEGFA expression in endocrine cells and associated receptor KDR highly expressed in endothelial cells. Transcripts encoding ECM components, including integrins, collagens, and laminins, were detected at high levels in pooled islet endothelial cells from both species, as well as single stellate cells from human islets (**Fig. 1h**).

Nerve fiber densities were 15-fold greater, and nerve fiber lengths were 63-fold greater in mouse compared to human (**Fig. 2a-b**). In contrast, human acinar tissue had a greater nerve fiber density and length when compared to mouse **(Fig. 2d-f**). Expression profiles of molecules that directly provide signals for axon growth, survival, and guidance cues, such as neurotrophic factors, ephrins, and semaphorins, and their associated receptors were relatively consistent between mouse and human islets, while SLIT/ROBO pathway components were detected at higher levels in mouse beta cells compared to human (**Fig. 2g**). Overall, the nerve fibers in the human pancreas were surprisingly more abundant and longer in acinar tissue than in islets (**Supplemental Fig. 3e-h**), and there were modest differences in neuronal signaling pathways by transcriptomic analysis (**Supplemental Fig. 5**). Additionally, percent capillary and nerve fiber area analyses revealed similar findings as described above (**Supplemental Fig. 4**). Our results demonstrate that the neurovascular architecture of islets and acinar tissue differs considerably between mouse and human supporting prior findings on pancreatic inter-species differences (17–19). We also showed that despite significant inter-species differences in islet neurovascular architecture, transcriptomic profiles of factors guiding angiogenesis and neuronal development in islets were quite similar, suggesting other cross-species regulatory relationships.

Capillary density is greater in islet and acinar tissue of recent-onset T1D. Utilizing the largest T1D cohort to date to assess neurovascular architecture, we investigated whether architectural changes are associated with or related to T1D disease duration. Because the

frequency of neuropathy increases with longer diabetes duration and the heterogeneity of T1D tissues, we subdivided a T1D donor cohort of 27 donors into two groups (**Fig. 3a**): 1) relatively recent-onset (< 10 years of disease) and 2) longstanding T1D (> 10 yrs of disease) (31). Recent-onset T1D donors had low but measurable C-peptide levels, whereas the levels in longstanding T1D donors were mostly below the detection limit (**Table 1**). Additionally, 33% (6 recent-onset; 3 longstanding) of these T1D donors were previously phenotyped for endocrine composition and/or islet function (31, 41, 42). The de-identified record of these donors did not specify whether the donors had autonomic or peripheral neuropathy (donor summary in **Table 1** and **Supplemental Table 1**).

The density of pancreatic capillaries, visualized by immunofluorescence labeling for caveolin-1 (CAV1) with 10 μm tissue sections, was greater in recent-onset T1D than in non-diabetic and longstanding T1D tissue in both pancreatic compartments (**Fig. 3b-d**), with no significant difference among anatomical regions (**Fig. 3e-h**). As with non-diabetic donors, T1D donors showed greater islet capillary density than in the acinar tissue (**Supplemental Fig. 3b, Supplemental Fig. 6a-b**), while area per capillary did not vary by T1D subgroup (**Fig. 3i-l**) or between the islet and acinar compartments (**Supplemental Fig. 3d, 6c-d**). Additionally, we found a negative correlation between the capillary density of islets (**Fig. 3f**) and acinar tissue (**Fig. 3h**) and age and disease duration in T1D donors. Quantification of percent capillary area revealed similar findings as described above (**Supplemental Fig. 7**).

Pancreatic islet and acinar nerve fibers persist in T1D. To investigate whether nerve fiber density is altered in T1D, we visualized all pancreatic nerve fibers with TUBB3. Genetic ablation of intra-islet capillaries through inactivation of a major angiogenic factor produced by β cells, vascular endothelial growth factor A (VEGF-A), leads to extensive islet nerve fiber loss, thus highlighting coordinated interactions between islet innervation and vasculature and the importance of studying these two islet compartments simultaneously (25). To our knowledge,

298 the simultaneous comparison of nerve fibers and capillaries has not been done at this scale in
299 human T1D tissues. Like non-diabetic pancreata, T1D nerve fibers projected from the acinar
300 compartment into islets but were less frequent within islets compared to acinar tissue (**Fig. 4**,
301 **Supplemental Videos 1-3**). Interestingly, fiber density in islets (**Fig. 4d**), but not acinar tissue
302 (**Fig. 4f**), was greater in both recent-onset and longstanding T1D when compared to non-
303 diabetic donor tissue. Acinar nerve fiber length did not differ among groups (**Fig. 4j**). Within
304 each group, both nerve fiber density and length were greater in acinar tissue compared to islets
305 (**Supplemental Fig. 3e-h, Supplemental Fig. 8a-b**). However, neither nerve fiber density nor
306 length correlated to donor age or T1D duration in either compartment (**Fig. 4e-i, 4g-k**).

307 **Sympathetic nerve fibers are similar in T1D and non-diabetic pancreata.** The autonomic
308 nervous system is important for initiating alpha cell response to hypoglycemia, particularly
309 through sympathetic fibers (1). Early loss of rodent sympathetic nerve fibers in models of T1D
310 has been hypothesized to lead to the dysregulation of glucagon secretion (12–14). Therefore,
311 we assessed T1D pancreatic sympathetic nerve fibers utilizing the marker tyrosine hydroxylase
312 (TH). In contrast to findings in T1D rodent models, we did not detect a change in sympathetic
313 islet or acinar fiber density in recent-onset or longstanding T1D (**Fig. 5**) (13, 14). In line with our
314 findings using the pan-neuronal marker TUBB3, the density and length of TH+ sympathetic
315 nerve fibers were greater in the acinar tissue compared to islets of both ND and T1D donors
316 (**Supplemental Fig. 8c**). Furthermore, sympathetic fibers predominated in the islet
317 compartment (**Supplemental Fig. 9a-b**) but made up only a subset of TUBB3+ pan-neuronal
318 fibers in the acinar compartment (**Supplemental Fig. 9c-d**). There was a negative correlation
319 between TH+ islet fiber density and length versus T1D cohort age but not the disease duration
320 (**Fig. 5e, 5i**). Quantification of percent nerve fiber area revealed similar findings as described
321 above (**Supplemental Fig. 10**).

Nerve fibers in islets and acinar tissue overlap with the extracellular matrix. The ECM is an essential part of the vasculature by providing structural blood vessel support and regulating vascular phenotype and function (43, 44). At the same time, it also regulates neuronal migration, the formation of axonal processes, and their function (43, 44). To understand the structural relationship between pancreatic nerve fibers, capillaries, and the ECM, we determined nerve fiber and ECM patterning in non-diabetic, recent-onset T1D, and longstanding T1D tissues. Three-dimensional (3D) reconstructions of TUBB3+ nerve fibers and ECM show that nerve fibers follow ECM within acinar tissue prior to extending into islets (**Fig. 6a-f, Supplemental Videos 1-3**). By visualizing capillaries, nerve fibers, and ECM with PECAM-1, TUBB3, and collagen IV (COLIV), respectively, we found that nerve fibers associated with the ECM in the acinar and islet compartments regardless of disease state (**Fig. 6a-f**). Our image analyses showed ~40% overlap of TUBB3+ nerve fiber area with COLIV+ ECM area (**Fig. 6g**). These results demonstrate that there is a strong spatial association between nerve fibers and ECM (**Fig. 6d', e', f'**), whereas, in acinar tissue, they follow ECM generated by acinar cells in areas devoid of capillaries (**Fig. 6d", e", f"**). Overall, these data indicate that pancreatic capillaries and nerve fibers persist in longstanding T1D (**Fig. 7**), contrasting with the loss of pancreatic innervation in rodent T1D models and thus emphasizing potentially distinct mechanisms of intrinsic alpha cell defects in dysregulated human glucagon secretion.

Data supplements can be accessed here:

- Supplemental Information: https://doi.org/10.6084/m9.figshare.21824502
- Supplemental Video 1: https://doi.org/10.6084/m9.figshare.21111625
- Supplemental Video 2: https://doi.org/10.6084/m9.figshare.21111622
- Supplemental Video 3: https://doi.org/10.6084/m9.figshare.21111628

347

DISCUSSION

Hypoglycemia is a major limitation of insulin therapy in T1D, and impaired glucagon secretion is a major contributor. Using bio-banked pancreatic tissues from T1D donors that spanned a wide range of diabetes duration, we investigated if impaired glucagon secretion could be attributed, at least in part, to the reduced islet innervation as suggested by studies in rodent models of T1D. To understand changes in the neurovascular architecture of human T1D pancreatic tissue, we systematically assessed innervation and vascularization in both islet and acinar tissue compartments of recent-onset and longstanding T1D donors and age-matched controls. As part of this study, we also analyzed the neurovascular architecture in mouse pancreas, a widely used model of human disease, and compared it to that of non-diabetic human controls. We found that human islets are much less vascularized and innervated than mouse islets (more than a 15-fold difference). In contrast to mouse islets, human islets are less innervated compared to surrounding acinar tissue. Human islets have fewer intra-islet capillaries with sparse nerve fibers, with these in close association with ECM. We also found that both nerve fibers and capillaries were present with greater capillary density in recent-onset T1D islets and acinar tissue. Surprisingly, we found that islet innervation was similar in T1D donors and controls, indicating that the islet neurovascular structures persist and are relatively unchanged in human T1D. These results, in conjunction with reports from others, suggest the need for alternative hypotheses other than reduced innervation to explain the dysregulated glucagon secretion in human T1D (18–20, 45).

The mechanisms responsible for the marked difference in vascularization and innervation in the mouse and human pancreas are unknown. Since in islets, innervation is tightly linked to vascularization with the vascular network generating an ECM scaffold for nerve fiber migration (26), one possible explanation is that greater vascularization in the mouse islets promotes greater innervation. This could explain the difference in innervation patterns between mouse

and human islets. Our comparative analysis of transcriptome data available for mouse and human islet endocrine and endothelial cells found overall similar transcriptomic profiles of factors guiding angiogenesis and neuronal development in islets suggesting other regulatory mechanisms, including possibly post-transcriptional processes (25, 26, 43, 46–49). For example, the generation of different isoforms of a master regulator of islet vascularization, VEGF-A, by alternative splicing (46) across different species could lead to isoforms with varying levels of activity due to their regulation by ECM, which could further influence growth factor availability, islet vascularization, and morphogenesis (20, 50–54). Because vascularization and innervation are complex processes, it is also possible that a combinatorial difference in the ligand-receptor expression could yield different neurovascular patterning between mouse and human. Alternatively, stromal and/or immune cells could further modulate signaling in a species-specific manner during the development of neurovascular assembly (55, 56). Furthermore, the greater innervation in the human exocrine compartment compared to the mouse indicates that the degree of innervation and vascularization is not always linked (25, 26, 43, 46–49). The inter-species differences in islet vascularization and innervation are reminiscent of other differences, such as islet cell composition and spatial arrangement, basement membrane organization, proliferative capacity, and basal insulin secretion, but the responsible molecular mechanisms for these are also not well-defined underscoring the caution when translating findings from model systems to human disease (50, 51, 57, 58).

Although the fundamental ability of the autonomic nervous system to activate pancreatic secretion is present in mice and humans, each species may integrate and respond to these signals differently (2–4). Rodent models of T1D show an early loss of islet nerve fiber density dependent on the degree of insulitis, suggesting a role for the immune system in perturbing these structures in conjunction with targeting beta cells (13, 14, 59) leading to an impaired sympathetic nerve fiber activation of glucagon secretion (14). In human T1D tissues, we did not

detect a reduction or loss of sympathetic nerve fibers. Instead, we found the persistence of these nerve fibers in islets. These differences between human and rodent models may be due to inter-species differences in the islet-related T1D pathogenesis with much more profound insulitis in NOD mice compared to human (2–4, 23, 59). Other nerve fiber type densities not assessed here due to reagent availability, such as parasympathetic or sensory nerves, may also change and influence secretion dysfunction seen in T1D (24, 60). Furthermore, a previous study found differences in the islet microvasculature between T1D insulin-positive and insulin-negative islets which we did not capture in the current study due to our immunolabeling paradigms (28). Additionally, an upregulation in vascular gene sets such as angiogenesis and blood vessel morphogenesis found in T1D islets (61) parallels the histological capillary changes reported in our current study. Therefore, the heterogeneous nature of β cell loss across T1D islets may lead to variabilities in T1D islet microvasculature and nerve fiber densities which need to be further studied (28). Overall, our studies of many human tissues do not support the hypothesis that glucagon secretion defects in T1D result from decreased islet sympathetic nerve fiber density.

Some differences exist between our findings and prior reports, including tissue thickness, the number of donors assessed, and nerve fiber markers utilized. One experimental difference is that we utilized both thin (10 μm) and thick (30 μm) cryosections from human tissue that were gently fixed to maximally preserve cellular and anatomical structures. Compared to optically cleared sections, 10 μm sections do not always capture the full length of some nerve fibers or capillaries. In contrast to much thicker optically cleared tissue sections, though, 10 μm sections allowed for high throughput morphometric analysis of ~3400 islets in total from a unique bio-banked cohort of 38 non-diabetic and T1D donors. We sought to circumvent this limitation by studying a tremendous number of islets from a large cohort of donors. Our high throughput analysis also allowed us to overcome high variability in human samples, particularly in T1D donor tissues. Other differences between this and other studies may be due to donor variability,

sample size, and/or technical differences during tissue handling, which may affect the downstream quantification of delicate structures such as nerve fibers. We used the pan-neuronal marker, TUBB3, while others have used neural cell adhesion molecule 1 (NCAM), neurofilament 200 (NF200), and ubiquitin carboxyl-terminal hydrolase isozyme (UCHL1 or PGP9.5) (17, 23, 60, 62) with a similar distribution of nerve fibers in human islets and acinar tissue when compared to PGP9.5 maker, thus further underscoring the appropriate utilization of TUBB3 in this study (62). It is important to note that TUBB3+ intrapancreatic ganglia could not be identified in either full-section confocal images or over 1,000 whole-slide images that we used for our high-throughput analyses. Therefore, nerve fiber bundles served as a positive control for TUBB3 immunolabeling of pancreatic nerve fibers in our study. Additionally, we used the sympathetic nerve fiber marker, TH, that labels throughout the axon to the nerve terminal and allows direct comparison to other studies utilizing this same marker.

The preservation of neurovascular architecture in T1D islets suggests other explanations for impaired glucagon secretion, such as intrinsic nerve fiber or capillary dysfunction and/or an intrinsic alpha cell defect. Recent studies using isolated islets and tissues from the same organ donors provide significant support for intrinsic alpha cell defect in T1D at both molecular and functional levels showing that impaired glucagon secretion was associated with reduced expression of key alpha cell-enriched regulators, including transcription factors *MAFB* and *ARX* and pointing to changes in metabolic pathways related to glycolysis and oxidative phosphorylation (31, 41, 63). While we show that neurovascular architecture is preserved in T1D, one cannot exclude an islet nerve fiber or capillary dysfunction, which are far more difficult to elucidate in human. For example, hyperglycemia could cause neurotransmitter receptor oxidation and reduced acetylcholine receptor activity in sympathetic neurons (64). Conversely, hypoglycemia sensed in the brain promotes counterregulatory responses from the adrenal gland and alpha cells. Dysfunctional CNS hypoglycemia-sensing in T1D could disrupt sympathetic

448 activation in islets, further impairing glucagon secretion (65). Given prior findings that
449 sympathetic nerve fibers preferentially innervate smooth muscle cells within the islet, disruptions
450 in the autonomic modulation of intra-islet vascular contractile components in T1D may also
451 contribute to diminished glucagon secretion during hypoglycemia (66). The recent development
452 of pancreatic slice physiology, which preserves vascular cytoarchitecture, highlighted the
453 importance of islet pericytes in modulating local vasodilation and constriction (33, 67).

454 Additional research is needed to determine whether the dysregulated glucagon secretion in T1D
455 results primarily from alpha cell-intrinsic defect and whether it is further compounded by
456 neuronal dysfunction. It is important that such studies examine a broad range of T1D duration
457 since mechanisms may differ with disease stages. New technologies, approaches, and models
458 to probe neurovascular function in islets are emerging, and these include the islet-on-a-chip
459 platform, pancreatic slices, islet transplantation models, and new imaging approaches (68–72).
460 For example, examining in vivo the processes of both innervation and vascularization of human
461 islets transplanted into immunodeficient mice may provide insights into the molecular
462 mechanisms of such processes.

ACKNOWLEDGEMENTS

We thank the organ donors and their families for their invaluable donations and the International Institute for Organ Procurement Organizations, Advancement of Medicine (IIAM), and the National Disease Research Exchange (NDRI) for their partnership in studies of human pancreatic tissue for research. This work was supported by the Human Islet Research Network (RRID:SCR_014393), the Human Pancreas Analysis Program (RRID:SCR_016202), DK106755, DK123716, DK123743, DK120456, DK104211, DK108120, DK112232, DK117147, DK112217, EY032442, DK20593 (Vanderbilt Diabetes Research and Training Center), The Leona M. and Harry B. Helmsley Charitable Trust, JDRF, the U.S. Department of Veterans Affairs (BX000666), and the National Science Foundation Graduate Research Fellowship (1937963). Whole-slide imaging was performed in the Islet and Pancreas Analysis Core of the Vanderbilt DRTC (DK20593). Some confocal imaging studies were performed in part through the Vanderbilt Cell Imaging Shared Resource (supported by NIH grants CA68485, DK20593, DK58404, DK59637, and EY08126). The graphical abstract was made, in part, with BioRender.com.

AUTHOR CONTRIBUTIONS

T.M.R., D.C.S., R.H., A.C.P., and M.B conceptualized and designed the study. T.M.R., R.H., R.B.R., J.P., and R.A. performed experiments. R.B., R.A., A.M.B., R.J., and HPAP were responsible for tissue acquisition and handling. T.M.R. and D.C.S. prepared figures. T.M.R., D.C.S., S.S., J-P.C, S.P., and H.K. performed analyses. T.M.R., D.C.S., A.C., A.C.P., and M.B. wrote the manuscript. All authors read and approved the manuscript. A.C.P. and M.B. are the guarantors of this work and, as such, had full access to all the data in the study and take responsibility for the integrity of the data and the accuracy of the data analysis.

DUALITY OF INTEREST

No potential conflicts of interest are relevant to this article were reported.

REFERENCES

1. Faber CL, Deem JD, Campos CA, Taborsky GJ, Morton GJ. CNS control of the endocrine pancreas. *Diabetologia* 63: 2086–2094, 2020. doi: 10.1007/s00125-020-05204-6.

2. Ahrén B, Holst JJ. The cephalic insulin response to meal ingestion in humans is dependent on both cholinergic and noncholinergic mechanisms and is important for postprandial glycemia. *Diabetes* 50: 1030--1038, 2001. doi: 10.2337/diabetes.50.5.1030.

3. Ahrén B. Autonomic regulation of islet hormone secretion--implications for health and disease. *Diabetologia* 43: 393--410, 2000. doi: 10.1007/s001250051322.

4. Havel PJ, Ahren B. Activation of Autonomic Nerves and the Adrenal Medulla Contributes to Increased Glucagon Secretion During Moderate Insulin-Induced Hypoglycemia in Women. 1997.

5. Hampton RF, Jimenez-Gonzalez M, Stanley SA. Unravelling innervation of pancreatic islets. *Diabetologia* 65: 1069–1084, 2022. doi: 10.1007/s00125-022-05691-9.

6. Gerich JE, Langlois M, Noacco C, Karam JH, Forsham PH. Lack of Glucagon Response to Hypoglycemia in Diabetes: Evidence for an Intrinsic Pancreatic Alpha Cell Defect. *Science* 182: 171–173, 1973. doi: 10.1126/science.182.4108.171.

7. Bolli G, Feo PD, Compagnucci P, Cartechini MG, Angeletti G, Santeusanio F, Brunetti P, Gerich JE. Abnormal Glucose Counterregulation in Insulin-dependent Diabetes Mellitus: Interaction of Anti-Insulin Antibodies and Impaired Glucagon and Epinephrine Secretion. *Diabetes* 32: 134–141, 1983. doi: 10.2337/diab.32.2.134.

8. Brown RJ, Sinaii N, Rother KI. Too much glucagon, too little insulin: time course of pancreatic islet dysfunction in new-onset type 1 diabetes. *Diabetes Care* 31: 1403–4, 2008. doi: 10.2337/dc08-0575.

9. Sherr J, Tsalikian E, Fox L, Buckingham B, Weinzimer S, Tamborlane WV, White NH, Arbelaez AM, Kollman C, Ruedy KJ, Cheng P, Beck RW, (DirecNet) for the DR in CN. Evolution of Abnormal Plasma Glucagon Responses to Mixed-Meal Feedings in Youth With Type 1 Diabetes During the First 2 Years After Diagnosis. *Diabetes Care* 37: 1741–1744, 2014. doi: 10.2337/dc13-2612.

10. Longo DL, Cryer PE. Mechanisms of Hypoglycemia-Associated Autonomic Failure in Diabetes. *New Engl J Medicine* 369: 362–372, 2013. doi: 10.1056/nejmra1215228.

11. Taborsky GJ, Ahrén B, Havel PJ. Autonomic mediation of glucagon secretion during hypoglycemia: implications for impaired alpha-cell responses in type 1 diabetes. *Diabetes* 47: 995–1005, 1998. doi: 10.2337/diabetes.47.7.995.

12. Mei Q, Mundinger TO, Lernmark A, Taborsky GJ. Early, selective, and marked loss of sympathetic nerves from the islets of BioBreeder diabetic rats. *Diabetes* 51: 2997--3002, 2002. doi: 10.2337/diabetes.51.10.2997.

524 13. Mundinger TO, Mei Q, Figlewicz DP, Lernmark Aa, Taborsky GJ. Impaired glucagon
525 response to sympathetic nerve stimulation in the BB diabetic rat: effect of early sympathetic islet
526 neuropathy. *Am J Physiol-endoc M* 285: E1047--E1054, 2003. doi:
527 10.1152/ajpendo.00136.2003.

528 14. Taborsky GJ, Mei Q, Hackney DJ, Figlewicz DP, Leboeuf R, Mundinger TO. Loss of islet
529 sympathetic nerves and impairment of glucagon secretion in the NOD mouse: Relationship to
530 invasive insulitis. *Diabetologia* 52: 2602--2611, 2009. doi: 10.1007/s00125-009-1494-5.

531 15. Tominaga M, Maruyama H, Vasko MR, Baetens D, Orci L, Unger RH. Morphologic and
532 Functional Changes in Sympathetic Nerve Relationships With Pancreatic α-Cells After
533 Destruction of β-Cells in Rats. *Diabetes* 36: 365–373, 1987. doi: 10.2337/diab.36.3.365.

534 16. Persson-Sj"ogren S, Holmberg D, Forsgren S. Remodeling of the innervation of pancreatic
535 islets accompanies insulitis preceding onset of diabetes in the NOD mouse. *J Neuroimmunol*
536 158: 128--137, 2005. doi: 10.1016/j.jneuroim.2004.08.019.

537 17. Alvarsson A, Jimenez-Gonzalez M, Li R, Rosselot C, Tzavaras N, Wu Z, Stewart AF,
538 Garcia-Ocaña A, Stanley SA. A 3D atlas of the dynamic and regional variation of pancreatic
539 innervation in diabetes. *Sci Adv* 6: eaaz9124, 2020. doi: 10.1126/sciadv.aaz9124.

540 18. Rodriguez-Diaz R, Abdulreda MH, Formoso A, Gans I, Ricordi C, Berggren PO, Caicedo A.
541 Innervation patterns of autonomic axons in the human endocrine pancreas. *Cell Metab* 14: 45--
542 54, 2011. doi: 10.1016/j.cmet.2011.05.008.

543 19. Tang S-C, Shen C-N, Lin P-Y, Peng S-J, Chien H-J, Chou Y-H, Chamberlain CE, Pasricha
544 PJ. Pancreatic neuro-insular network in young mice revealed by 3D panoramic histology.
545 *Diabetologia* 61: 158–167, 2018. doi: 10.1007/s00125-017-4408-y.

546 20. Brissova M, Shostak A, Fligner CL, Revetta FL, Washington MK, Powers AC, Hull RL.
547 Human Islets Have Fewer Blood Vessels than Mouse Islets and the Density of Islet Vascular
548 Structures Is Increased in Type 2 Diabetes. *J Histochem Cytochem* 63: 637--645, 2015. doi:
549 10.1369/0022155415573324.

550 21. Otonkoski T, Banerjee M, Korsgren O, Thornell L -E., Virtanen I. Unique basement
551 membrane structure of human pancreatic islets: implications for β-cell growth and differentiation.
552 *Diabetes Obes Metabolism* 10: 119–127, 2008. doi: 10.1111/j.1463-1326.2008.00955.x.

553 22. Mundinger TO, Mei Q, Foulis AK, Fligner CL, Hull RL, Taborsky GJ. Human Type 1
554 Diabetes Is Characterized by an Early, Marked, Sustained, and Islet-Selective Loss of
555 Sympathetic Nerves. *Diabetes* 65: 2322–2330, 2016. doi: 10.2337/db16-0284.

556 23. Campbell-Thompson M, Butterworth EA, Boatwright JL, Nair MA, Nasif LH, Nasif K, Revell
557 AY, Riva A, Mathews CE, Gerling IC, Schatz DA, Atkinson MA. Islet sympathetic innervation
558 and islet neuropathology in patients with type 1 diabetes. *Sci Rep-uk* 11: 6562, 2021. doi:
559 10.1038/s41598-021-85659-8.

560 24. Lundberg M, Lindqvist A, Wierup N, Krogvold L, Dahl-Jørgensen K, Skog O. The density of
561 parasympathetic axons is reduced in the exocrine pancreas of individuals recently diagnosed
562 with type 1 diabetes. *Plos One* 12: e0179911, 2017. doi: 10.1371/journal.pone.0179911.

25. Reinert RB, Brissova M, Shostak A, Pan FC, Poffenberger G, Cai Q, Hundemer GL, Kantz J, Thompson CS, Dai C, McGuinness OP, Powers AC. Vascular Endothelial Growth Factor-A and Islet Vascularization Are Necessary in Developing, but Not Adult, Pancreatic Islets. *Diabetes* 62: 4154–4164, 2013. doi: 10.2337/db13-0071.

26. Reinert RB, Cai Q, Hong J-Y, Plank JL, Aamodt K, Prasad N, Aramandla R, Dai C, Levy SE, Pozzi A, Labosky PA, Wright CVE, Brissova M, Powers AC. Vascular endothelial growth factor coordinates islet innervation via vascular scaffolding. *Development* 141: 1480–1491, 2014. doi: 10.1242/dev.098657.

27. Plank JL, Mundell NA, Frist AY, LeGrone AW, Kim T, Musser MA, Walter TJ, Labosky PA. Influence and timing of arrival of murine neural crest on pancreatic beta cell development and maturation. *Dev Biol* 349: 321–330, 2011. doi: 10.1016/j.ydbio.2010.11.013.

28. Canzano JS, Nasif LH, Butterworth EA, Fu DA, Atkinson MA, Campbell-Thompson M. Islet Microvasculature Alterations With Loss of Beta-cells in Patients With Type 1 Diabetes. *J Histochem Cytochem* 67: 41--52, 2018. doi: 10.1369/0022155418778546.

29. Campbell-Thompson ML, Filipp SL, Grajo JR, Nambam B, Beegle R, Middlebrooks EH, Gurka MJ, Atkinson MA, Schatz DA, Haller MJ. Relative Pancreas Volume Is Reduced in First-Degree Relatives of Patients With Type 1 Diabetes. *Diabetes Care* 42: 281–287, 2018. doi: 10.2337/dc18-1512.

30. Wright JJ, Saunders DC, Dai C, Poffenberger G, Cairns B, Serreze DV, Harlan DM, Bottino R, Brissova M, Powers AC. Decreased pancreatic acinar cell number in type 1 diabetes. .

31. Brissova M, Haliyur R, Saunders D, Shrestha S, Dai C, Blodgett DM, Bottino R, Campbell-Thompson M, Aramandla R, Poffenberger G, Lindner J, Pan FC, Herrath MG von, Greiner DL, Shultz LD, Sanyoura M, Philipson LH, Atkinson M, Harlan DM, Levy SE, Prasad N, Stein R, Powers AC. α Cell Function and Gene Expression Are Compromised in Type 1 Diabetes. *Cell Reports* 22: 2601--2614, 2018. doi: 10.1016/j.celrep.2018.02.032.

32. Haliyur R, Tong X, Sanyoura M, Shrestha S, Lindner J, Saunders DC, Aramandla R, Poffenberger G, Redick SD, Bottino R, Prasad N, Levy SE, Blind RD, Harlan DM, Philipson LH, Stein RW, Brissova M, Powers AC. Human islets expressing HNF1A variant have defective β cell transcriptional regulatory networks. *J Clin Invest* 129: 246–251, 2018. doi: 10.1172/jci121994.

33. Almac J, Weitz J, Rodriguez-diaz R, Pereira E, Caicedo A, ro, Almac J. The Pericyte of the Pancreatic Islet Regulates Capillary Diameter and Local Blood Flow Article. *Cell Metab* 27: 1--15, 2018. doi: 10.1016/j.cmet.2018.02.016.

34. Saunders DC, Aamodt KI, Richardson TM, Hopkirk AJ, Aramandla R, Poffenberger G, Jenkins R, Flaherty DK, Prasad N, Levy SE, Powers AC, Brissova M. Coordinated interactions between endothelial cells and macrophages in the islet microenvironment promote β cell regeneration. *Npj Regen Medicine* 6: 22, 2021. doi: 10.1038/s41536-021-00129-z.

35. Tweedie S, Braschi B, Gray K, Jones TEM, Seal RL, Yates B, Bruford EA. Genenames.org: the HGNC and VGNC resources in 2021. *Nucleic Acids Res* 49: gkaa980-, 2020. doi: 10.1093/nar/gkaa980.

603 36. Jonsson A, Hedin A, Müller M, Skog O, Korsgren O. Transcriptional profiles of human islet
604 and exocrine endothelial cells in subjects with or without impaired glucose metabolism. *Sci Rep-*
605 *uk* 10: 22315, 2020. doi: 10.1038/s41598-020-79313-y.

606 37. Walker JT, Saunders DC, Rai V, Dai C, Orchard P, Hopkirk AL, Reihsmann CV, Tao Y, Fan
607 S, Shrestha S, Varshney A, Wright JJ, Pettway YD, Ventresca C, Agarwala S, Aramandla R,
608 Poffenberger G, Jenkins R, Hart NJ, Greiner DL, Shultz LD, Bottino R, Program HPA, Liu J,
609 Parker SCJ, Powers AC, Brissova M. RFX6-mediated dysregulation defines human β cell
610 dysfunction in early type 2 diabetes. .

611 38. Erener S, Ellis CE, Ramzy A, Glavas MM, O'Dwyer S, Pereira S, Wang T, Pang J, Bruin JE,
612 Riedel MJ, Baker RK, Webber TD, Lesina M, Blüher M, Algül H, Kopp JL, Herzig S, Kieffer TJ.
613 Deletion of pancreas-specific miR-216a reduces beta-cell mass and inhibits pancreatic cancer
614 progression in mice. *Cell Reports Medicine* 2: 100434, 2021. doi: 10.1016/j.xcrm.2021.100434.

615 39. Shrestha S, Saunders DC, Walker JT, Camunas-Soler J, Dai X-Q, Haliyur R, Aramandla R,
616 Poffenberger G, Prasad N, Bottino R, Stein R, Cartailler J-P, Parker SCJ, MacDonald PE, Levy
617 SE, Powers AC, Brissova M. Combinatorial transcription factor profiles predict mature and
618 functional human islet α and β cells. *JCI Insight* 6: e151621, 2021. doi:
619 10.1172/jci.insight.151621.

620 40. Hao Y, Hao S, Andersen-Nissen E, Mauck WM, Zheng S, Butler A, Lee MJ, Wilk AJ, Darby
621 C, Zager M, Hoffman P, Stoeckius M, Papalexi E, Mimitou EP, Jain J, Srivastava A, Stuart T,
622 Fleming LM, Yeung B, Rogers AJ, McElrath JM, Blish CA, Gottardo R, Smibert P, Satija R.
623 Integrated analysis of multimodal single-cell data. *Cell* 184: 3573-3587.e29, 2021. doi:
624 10.1016/j.cell.2021.04.048.

625 41. Doliba NM, Rozo AV, Roman J, Qin W, Traum D, Gao L, Liu J, Manduchi E, Liu C, Golson
626 ML, Vahedi G, Naji A, Matschinsky FM, Atkinson MA, Powers AC, Brissova M, Kaestner KH,
627 Stoffers DA, Consortium H. α Cell dysfunction in islets from nondiabetic, glutamic acid
628 decarboxylase autoantibody–positive individuals. *J Clin Investigation* 132: e156243, 2022. doi:
629 10.1172/jci156243.

630 42. Damond N, Engler S, Zanotelli VRT, Schapiro D, Wasserfall CH, Kusmartseva I, Nick HS,
631 Thorel F, Herrera PL, Atkinson MA, Bodenmiller B. A Map of Human Type 1 Diabetes
632 Progression by Imaging Mass Cytometry. *Cell Metab* 29: 755-768.e5, 2019. doi:
633 10.1016/j.cmet.2018.11.014.

634 43. Myers JP, Santiago-Medina M, Gomez TM. Regulation of axonal outgrowth and pathfinding
635 by integrin–ecm interactions. *Dev Neurobiol* 71: 901–923, 2011. doi: 10.1002/dneu.20931.

636 44. Nikolova G, Jabs N, Konstantinova I, Domogatskaya A, Tryggvason K, Sorokin L, Fässler R,
637 Gu G, Gerber H-P, Ferrara N, Melton DA, Lammert E. The Vascular Basement Membrane: A
638 Niche for Insulin Gene Expression and β Cell Proliferation. *Dev Cell* 10: 397–405, 2006. doi:
639 10.1016/j.devcel.2006.01.015.

640 45. Chiu YC, Hua TE, Fu YY, Pasricha PJ, Tang SC. 3-D imaging and illustration of the
641 perfusive mouse islet sympathetic innervation and its remodelling in injury. *Diabetologia* 55:
642 3252--3261, 2012. doi: 10.1007/s00125-012-2699-6.

643 46. Carmeliet P, Tessier-Lavigne M. Common mechanisms of nerve and blood vessel wiring.
644 *Nature* 436: 193–200, 2005. doi: 10.1038/nature03875.

645 47. Brissova M, Shostak A, Shiota M, Wiebe PO, Poffenberger G, Kantz J, Chen Z, Carr C,
646 Jerome WG, Chen J, Baldwin HS, Nicholson W, Bader DM, Jetton T, Gannon M, Powers AC.
647 Pancreatic Islet Production of Vascular Endothelial Growth Factor-A Is Essential for Islet
648 Vascularization, Revascularization, and Function. *Diabetes* 55: 2974–2985, 2006. doi:
649 10.2337/db06-0690.

650 48. Cai Q, Brissova M, Reinert RB, Pan FC, Brahmachary P, Jeansson M, Shostak A, Radhika
651 A, Ia, Poffenberger G, Quaggin SE, Jerome WG, Dumont DJ, Powers AC. Enhanced expression
652 of VEGF-A in B cells increases endothelial cell number but impairs islet morphogenesis and B
653 cell proliferation. *Dev Biol* 367: 40--54, 2012. doi: 10.1016/j.ydbio.2012.04.022.

654 49. Adams RH, Eichmann A. Axon Guidance Molecules in Vascular Patterning. *Csh Perspect*
655 *Biol* 2: a001875, 2010. doi: 10.1101/cshperspect.a001875.

656 50. Brissova M, Fowler MJ, Nicholson WE, Chu A, Hirshberg B, Harlan DM, Powers AC.
657 Assessment of human pancreatic islet architecture and composition by laser scanning confocal
658 microscopy. *J Histochem Cytochem* 53: 1087--1097, 2005. doi: 10.1369/jhc.5c6684.2005.

659 51. Cabrera O, Berman DM, Kenyon NS, Ricordi C, Berggren P-O, Caicedo A. The unique
660 cytoarchitecture of human pancreatic islets has implications for islet cell function. *P Natl Acad*
661 *Sci Usa* 103: 2334–2339, 2006. doi: 10.1073/pnas.0510790103.

662 52. Dolenšek J, Rupnik MS, Stožer A. Structural similarities and differences between the human
663 and the mouse pancreas. *Islets* 7: e1024405, 2015. doi: 10.1080/19382014.2015.1024405.

664 53. Korpos E, Kadri N, Kappelhoff R, Wegner J, Overall CM, Weber E, Holmberg D, Cardell S,
665 Sorokin L. The Peri-islet Basement Membrane, a Barrier to Infiltrating Leukocytes in Type 1
666 Diabetes in Mouse and Human. *Diabetes* 62: 531–542, 2012. doi: 10.2337/db12-0432.

667 54. Otonkoski T, Banerjee M, Korsgren O, Thornell L -E., Virtanen I. Unique basement
668 membrane structure of human pancreatic islets: implications for β-cell growth and differentiation.
669 *Diabetes Obes Metabolism* 10: 119–127, 2008. doi: 10.1111/j.1463-1326.2008.00955.x.

670 55. Hajizadeh-Saffar E, Tahamtani Y, Aghdami N, Azadmanesh K, Habibi-Anbouhi M,
671 Heremans Y, Leu ND, Heimberg H, Ravassard P, Shokrgozar MA, Baharvand H. Inducible
672 VEGF expression by human embryonic stem cell-derived mesenchymal stromal cells reduces
673 the minimal islet mass required to reverse diabetes. *Sci Rep-uk* 5: 9322, 2015. doi:
674 10.1038/srep09322.

675 56. Ghezelayagh Z, Zabihi M, Ashtiani MK, Ghezelayagh Z, Lynn FC, Tahamtani Y.
676 Recapitulating pancreatic cell–cell interactions through bioengineering approaches: the
677 momentous role of non-epithelial cells for diabetes cell therapy. *Cell Mol Life Sci* 78: 7107–
678 7132, 2021. doi: 10.1007/s00018-021-03951-2.

679 57. Virtanen I, Banerjee M, Palgi J, Korsgren O, Lukinius A, Thornell LE, Kikkawa Y, Sekiguchi
680 K, Hukkanen M, Konttinen YT, Otonkoski T. Blood vessels of human islets of Langerhans are

surrounded by a double basement membrane. *Diabetologia* 51: 1181--1191, 2008. doi: 10.1007/s00125-008-0997-9.

58. Dai C, Brissova M, Hang Y, Thompson C, Poffenberger G, Shostak A, Chen Z, Stein R, Powers AC. Islet-enriched gene expression and glucose-induced insulin secretion in human and mouse islets. 2012.

59. Veld PI. Insulitis in human type 1 diabetes: a comparison between patients and animal models. *Semin Immunopathol* 36: 569–579, 2014. doi: 10.1007/s00281-014-0438-4.

60. Chien H-J, Chiang T-C, Peng S-J, Chung M-H, Chou Y-H, Lee C-Y, Jeng Y-M, Tien Y-W, Tang S-C. Human pancreatic afferent and efferent nerves: mapping and 3-D illustration of exocrine, endocrine, and adipose innervation. .

61. Granlund L, Hedin A, Korsgren O, Skog O, Lundberg M. Altered microvasculature in pancreatic islets from subjects with type 1 diabetes. *Plos One* 17: e0276942, 2022. doi: 10.1371/journal.pone.0276942.

62. Tang S-C, Baeyens L, Shen C-N, Peng S-J, Chien H-J, Scheel DW, Chamberlain CE, German MS. Human pancreatic neuro-insular network in health and fatty infiltration. *Diabetologia* 61: 168–181, 2018. doi: 10.1007/s00125-017-4409-x.

63. Chakravarthy H, Gu X, Enge M, Dai X, Wang Y, Damond N, Downie C, Liu K, Wang J, Xing Y, Chera S, Thorel F, Quake S, Oberholzer J, MacDonald PE, Herrera PL, Kim SK. Converting Adult Pancreatic Islet α Cells into β Cells by Targeting Both Dnmt1 and Arx. *Cell Metab* 25: 622–634, 2017. doi: 10.1016/j.cmet.2017.01.009.

64. Campanucci V, Krishnaswamy A, Cooper E. Diabetes Depresses Synaptic Transmission in Sympathetic Ganglia by Inactivating nAChRs through a Conserved Intracellular Cysteine Residue. *Neuron* 66: 827–834, 2010. doi: 10.1016/j.neuron.2010.06.010.

65. Belfort-DeAguiar R, Gallezot J-D, Hwang JJ, Elshafie A, Yeckel CW, Chan O, Carson RE, Ding Y-S, Sherwin RS. Noradrenergic Activity in the Human Brain: A Mechanism Supporting the Defense Against Hypoglycemia. *J Clin Endocrinol Metabolism* 103: 2244–2252, 2018. doi: 10.1210/jc.2017-02717.

66. Rodriguez-Diaz R, Abdulreda MH, Formoso A, L. er, Gans I, Ricordi C, Berggren PO, Caicedo A. Innervation patterns of autonomic axons in the human endocrine pancreas. .

67. Gonçalves LM, Almaça J. Functional Characterization of the Human Islet Microvasculature Using Living Pancreas Slices. *Front Endocrinol* 11: 602519, 2021. doi: 10.3389/fendo.2020.602519.

68. Glieberman AL, Pope BD, Zimmerman JF, Liu Q, Ferrier JP, Kenty JHR, Schrell AM, Mukhitov N, Shores KL, Tepole AB, Melton DA, Roper MG, Parker KK. Synchronized stimulation and continuous insulin sensing in a microfluidic human Islet on a Chip designed for scalable manufacturing. *Lab Chip* 19: 2993–3010, 2019. doi: 10.1039/c9lc00253g.

69. Speier S, Rupnik M. A novel approach to in situ characterization of pancreatic β-cells. *Pflügers Archiv* 446: 553–558, 2003. doi: 10.1007/s00424-003-1097-9.

70. Speier S, Nyqvist D, Cabrera O, Yu J, Molano RD, Pileggi A, Moede T, Köhler M, Wilbertz J, Leibiger B, Ricordi C, Leibiger IB, Caicedo A, Berggren P-O. Noninvasive in vivo imaging of pancreatic islet cell biology. *Nat Med* 14: 574–578, 2008. doi: 10.1038/nm1701.

71. Rodriguez-Diaz R, Speier S, Molano RD, Formoso A, Gans I, Abdulreda MH, Cabrera O, Molina J, Fachado A, Ricordi C, Leibiger I, Pileggi A, Berggren P-O, Caicedo A. Noninvasive in vivo model demonstrating the effects of autonomic innervation on pancreatic islet function. *Proc National Acad Sci* 109: 21456–21461, 2012. doi: 10.1073/pnas.1211659110.

72. Morini S, Brown ML, Cicalese L, Elias G, Carotti S, Gaudio E, Rastellini C. Revascularization and remodelling of pancreatic islets grafted under the kidney capsule. *J Anat* 210: 565–577, 2007. doi: 10.1111/j.1469-7580.2007.00717.x.

730 **TABLES**

731 **Table 1. Overview of donor cohort characteristics.**

Donor Group	N	Age (years)	Disease Duration (years)	Sex (F / M)	BMI (kg/m²)	HbA1c (%)	C-peptide (ng/mL)
Non-diabetic	11	31 ± 15	N/A	3 / 11	30 ± 13	5.57 ± 0.30	13.18 ± 11.41
T1D Recent-onset (<10 yrs)	15	25 ± 14	6 ± 2	5 / 15	24 ± 6	9.49 ± 0.168	0.11 ± 0.13 (* vs. ND & T1D >10 yrs)
T1D Longstanding (>10 yrs)	12	45 ± 14	31 ± 11	3 / 12	27 ± 5	8.9 ± 1.45	< 0.02 or UD (* vs. ND & T1D <10 yrs)

732 Abbreviations: N, sample size; F, female; M, male; BMI, body mass index; HbA1c, Hemoglobin
733 A1c; T1D, type 1 diabetes; UD, undetectable. Averages are displayed with mean ± standard
734 deviation when applicable for non-diabetic and T1D donors. Asterisk (*) represents a statistically
735 significant p-value < 0.05 for comparisons between donor groups assessed by Mann-Whitney
736 tests. For statistical purposes, C-peptide values < 0.02 ng/mL (the lower limit of assay
737 detection) and undetectable C-peptide levels were set to 0. For T1D recent-onset, 4 donors had
738 C-peptide values < 0.02 ng/mL, and 3 donors had undetectable values. For T1D longstanding, 7
739 donors had C-peptide levels < 0.02 ng/mL, 4 donors had undetectable values. The T1D
740 longstanding donor with a C-peptide level of 1.78 was determined to be an outlier and excluded
741 from analyses.

FIGURE LEGENDS

Fig. 1. Human islets are less vascularized than mouse islets. Representative immunofluorescent staining (a-a', b-b') and quantification (c-f) of vasculature, as measured by endothelial cell staining (PECAM-1 or CAV1; magenta). Islets are visualized by hormones (insulin, INS; glucagon, GCG; green) and panels a' and b' show PECAM-1 or CAV1 only with islet area outlined. Scale bars, 100 μm. Quantification (mean ± s.e.m.) includes capillary density (panels c, d; left) and area per capillary (right) in islets (e) and acinar tissue (f) from mouse (grey; N = 5; 129 total islets, 127 total acinar measurements) and human (dark blue; N = 11; 488 total islets, 1392 total acinar measurements). Symbols on bar graphs represent individual mouse or human donors. Statistically significant p-values (< 0.05) are stated for Mann-Whitney tests. (g-h) Transcript levels of select angiogenic factors and receptors (g) and extracellular matrix (ECM) molecules (h) detected in islet endocrine cells, endothelial cells, and immune cells as measured by RNA-sequencing (RNA-seq). From top to bottom: mouse bulk datasets, Saunders et al. 2021; human bulk beta, Walker et al. 2021; human bulk endothelial, Jonsson et al. 2020; single-cell (sc) datasets: mouse, Erener et al. 2021; human, Shrestha et al. 2021. Boxed 'M' and 'H' label mouse and human datasets, respectively. Only values >0.2 (sc) and log2 >8 (bulk) are graphed. Normalized expression (NE) units vary by study; see Methods. EC, endothelial cell; Imm., immune; Stell., stellate; VEGF, vascular endothelial growth factor.

Fig. 2. Human islets are less innervated than mouse islets. Representative immunofluorescent staining (a-a', b-b') and quantification (c-f) of nerve fibers, as measured by tubulin beta 3 (TUBB3; white). Islets are visualized by hormones (insulin, INS; glucagon, GCG; green) and panels a' and b' show TUBB3 only with islet area outlined. Scale bars, 100 μm. Quantification (mean ± s.e.m.) includes TUBB3+ fiber density (c, d; left) and length (right) in islets (e) and acinar tissue (f) from mouse (N = 5; 128 total islets, 262 total acinar measurements) and human (N = 11; 547 total islets, 1830 total acinar measurements). Symbols

on bar graphs represent individual mouse or human donors. Statistically significant p-values (< 0.05) are stated for Mann-Whitney tests. (g) Transcript levels of select neuronal ligands and receptors as measured by RNA-sequencing (RNA-seq). From top to bottom: mouse bulk datasets, Saunders et al. 2021; human bulk beta (β), Walker et al. 2021; human bulk endothelial, Jonsson et al. 2020; single-cell (sc) datasets: mouse, Erener et al. 2021; human, Shrestha et al. 2021. Boxed 'M' and 'H' label mouse and human datasets, respectively. Neurotr. factors = neurotrophic factor genes. Only values >0.2 (sc) and log2 >8 (bulk) are graphed. Normalized expression (NE) units vary by study; see Methods. EC, endothelial cell; Imm., immune; Stell., stellate.

Fig. 3. Islets in recent-onset T1D have greater vascular density compared to controls. (a) Schematic illustrating donor classification and experimental approach. (b-d) Representative immunofluorescent staining of vasculature labeled with caveolin-1 (CAV1; magenta) in pancreatic tissue sections from non-diabetic (b), T1D recent-onset (c), and T1D longstanding (d) donors. Panels (b'-d') show insets of (b-d), CAV1 channel only, with islet area outlined. Scale bars, 100 μm. (e-l) Quantification (mean + s.e.m.) of capillary density (e-h) and area per capillary (i-l) in islet (e-j) and acinar (g-l) tissue from pancreata of non-diabetic (dark blue; N = 11; 488 total islets, 1392 total acinar measurements), T1D recent-onset (light blue; N = 14; 471 total islets, 1332 total acinar measurements), and T1D longstanding (light blue striped; N = 12; 316 total islets, 867 total acinar measurements) donors. Each symbol represents an individual donor; 'aggregate' graph values reflect the average data from all pancreas regions, which are stratified (H, Head; B, Body; T, Tail) to the right. Horizontal lines represent mean values and are colorized based on the donor group. (f) Islet and (h) acinar capillary density in ND and T1D tissue, plotted as a function of donor age and disease duration. (j) Islet and (l) acinar area per capillary in ND and T1D tissue, plotted as a function of donor age and disease duration. Statistically significant p-values (< 0.05) are stated for the following statistical tests: (e, i, g, k)

aggregate, Kruskal-Wallis One-Way ANOVA with Dunn's multiple comparisons tests; anatomical location, Mixed-effects One-Way ANOVA with Holm-Sidak's multiple comparison tests; (f-j, h-l) nonlinear regression analysis with lines of best fit and Spearman correlation r values denoted on each plot.

Fig. 4. Islets in T1D have greater nerve fiber density compared to controls. (a-c) Representative immunofluorescent staining of nerve fibers labeled with tubulin beta 3 (TUBB3; white) in pancreatic tissue sections from non-diabetic (a), T1D recent-onset (b), and T1D longstanding (d) donors. Panels (a'-c') show insets of (a-c), TUBB3 channel only, with islet area outlined. Scale bars, 100 μm. (d-k) Quantification (mean + s.e.m.) of nerve fiber density (d-g) and nerve fiber length (h-k) in islet (d-i) and acinar (f-k) tissue from pancreata of non-diabetic (dark blue; N = 11; 536 total islets, 1830 total acinar measurements), T1D recent-onset (light blue; N = 14; 417 total islets, 1258 total acinar measurements), and T1D longstanding (light blue striped; N = 11; 345 total islets, 1044 total acinar measurements) donors. Each symbol represents an individual donor; 'aggregate' graph values reflect the average data from all pancreas regions, which are stratified (H, Head; B, Body; T, Tail) to the right. Horizontal lines represent mean values and are colorized based on the donor group. (e) Islet and (g) acinar nerve fiber density in ND and T1D tissue, plotted as a function of donor age and disease duration. (i) Islet and (k) acinar nerve fiber length in ND and T1D tissue, plotted as a function of donor age and disease duration. Statistically significant p-values (< 0.05) are stated for the following statistical tests: (d, h, f, j) aggregate, Kruskal-Wallis One-Way ANOVA with Dunn's multiple comparisons tests; anatomical location, Mixed-effects One-Way ANOVA with Holm-Sidak's multiple comparison tests; (e, i, g, k) nonlinear regression analysis with lines of best fit and Spearman correlation r values denoted on each plot.

Fig. 5. Sympathetic nerve fibers are not reduced in human T1D islets compared to ND. (a-c) Representative immunofluorescent staining of sympathetic nerve fibers labeled with tyrosine

hydroxylase (TH; white) in pancreatic tissue sections from non-diabetic (a), T1D recent-onset (b), and T1D longstanding (c) donors. Panels (a'-c') show insets of (a-c), TH channel only, with islet area outlined. Scale bars, 100 μm. (d-k) Quantification (mean + s.e.m.) of sympathetic nerve fiber density (d-g) and nerve fiber length (h-k) in islet (d-i) and acinar (f-k) tissue from pancreata of non-diabetic (dark blue; N = 11; 514 total islets, 789 total acinar measurements), T1D recent-onset (light blue; N = 13; 469 total islets, 864 total acinar measurements), and T1D longstanding (light blue striped; N = 12; 325 total islets, 504 total acinar measurements) donors. Each symbol represents an individual donor; 'aggregate' graph values reflect the average data from all pancreas regions, which are stratified (H, Head; B, Body; T, Tail) to the right. Horizontal lines represent mean values and are colorized based on the donor group. (e) Islet and (g) acinar sympathetic nerve fiber density in ND and T1D tissue, plotted as a function of donor age and disease duration. (i) Islet and (k) acinar sympathetic nerve fiber length in ND and T1D tissue, plotted as a: (d, h, f, j) aggregate, Kruskal-Wallis One-Way ANOVA with Dunn's multiple comparisons tests; anatomical location, Mixed-effects One-Way ANOVA with Holm-Sidak's multiple comparison tests; (e, i, g, k) nonlinear regression analysis with lines of best fit and Spearman correlation r values denoted on each plot.

Fig. 6. Pancreatic nerve fibers associate with endothelial cell- or acinar cell-derived extracellular matrix (ECM) in human pancreatic tissue. (a-c) Representative images of pancreatic tissue from non-diabetic and T1D donors co-stained for nerves (TUBB3; white), ECM (COLIV; blue), and islets (INS/GCG; green). Insets (a'-c') show nerve fibers and ECM overlapping (white arrowheads) in both endocrine and exocrine compartments; the endocrine channel is removed for clarity. (d-f) Co-staining for nerves, ECM, and endothelial cells (PECAM-1; magenta). Insets from islet (d'-f') and acinar (d"-f") regions show nerve fibers and ECM overlapping with endothelial cells (yellow arrowheads); while white arrows distinguish regions where there is no overlap with the vasculature. Islets are outlined in white. Scale bars, 100 μm.

G) Quantification (mean + s.e.m.) of colocalization between nerve fibers (TUBB3+) and ECM (COLIV+) of islet and acinar tissue from non-diabetic (dark blue; N = 9; 35 total islets, 46 total acinar measurements), T1D recent-onset (light blue; N = 3; 11 total islets, 13 total acinar measurements), and T1D longstanding (light blue striped N = 6; 12 total islets, 19 total acinar measurements). Manders' overlap coefficients range between 0 and 1, in which 1 indicates 100% colocalization. P-values were calculated by paired Wilcoxon t-tests where ns indicates a p-value > 0.05.

Fig. 7. Human pancreatic neurovascular landscape in health and type 1 diabetes. The pancreas is intricately connected to the central nervous system and vasculature through branches of the autonomic nervous system and branching vessels. Nerve fibers and vessels can directly influence pancreatic function. Sympathetic projections originate in the spinal cord before extending through distal ganglia and intra-pancreatic ganglia. Islets (see inset; left) receive vascular and nerve fiber inputs that overlap with each other. Acinar tissue (see inset; right) is innervated and vascularized, with these components extending around acini. Pancreatic nerve fibers are associated with ECM laid down by either intra-islet vessels or acini. There exist inter-species and disease differences in the neurovascular patterns in the pancreas, as described by the summary table. The key denotes pertinent neuronal components (nerve soma and nerve terminals), capillaries, and extracellular matrix (ECM).

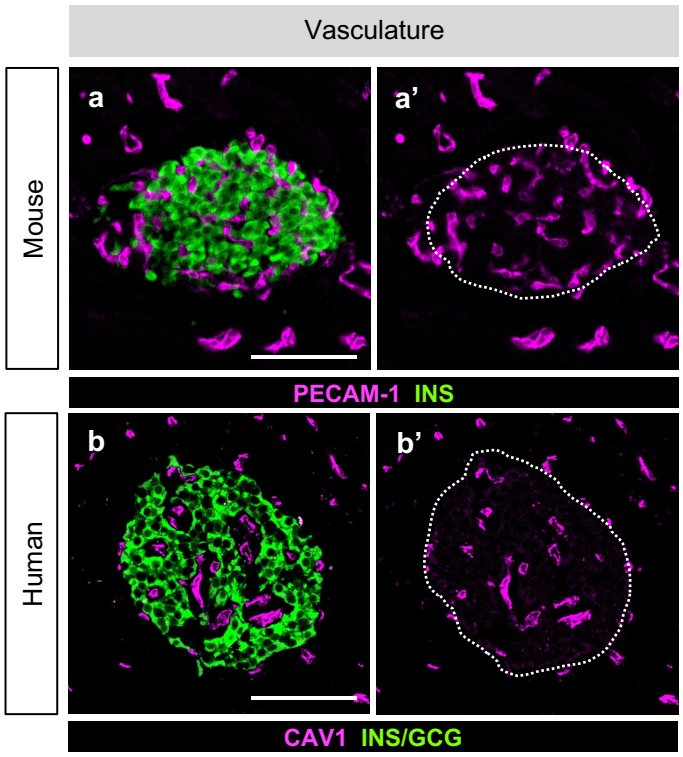

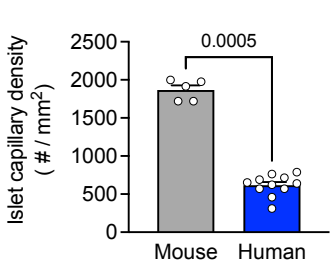

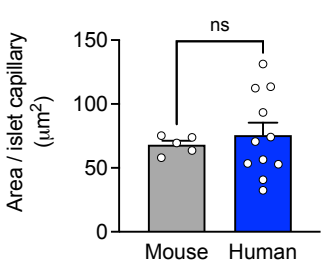

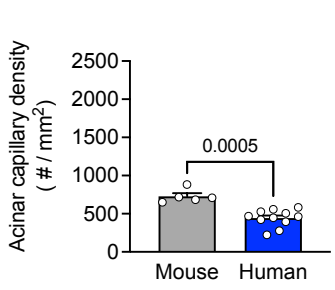

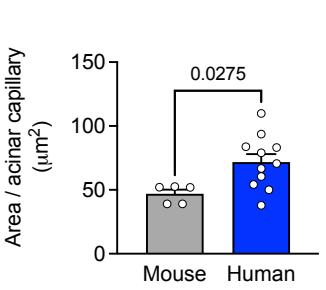

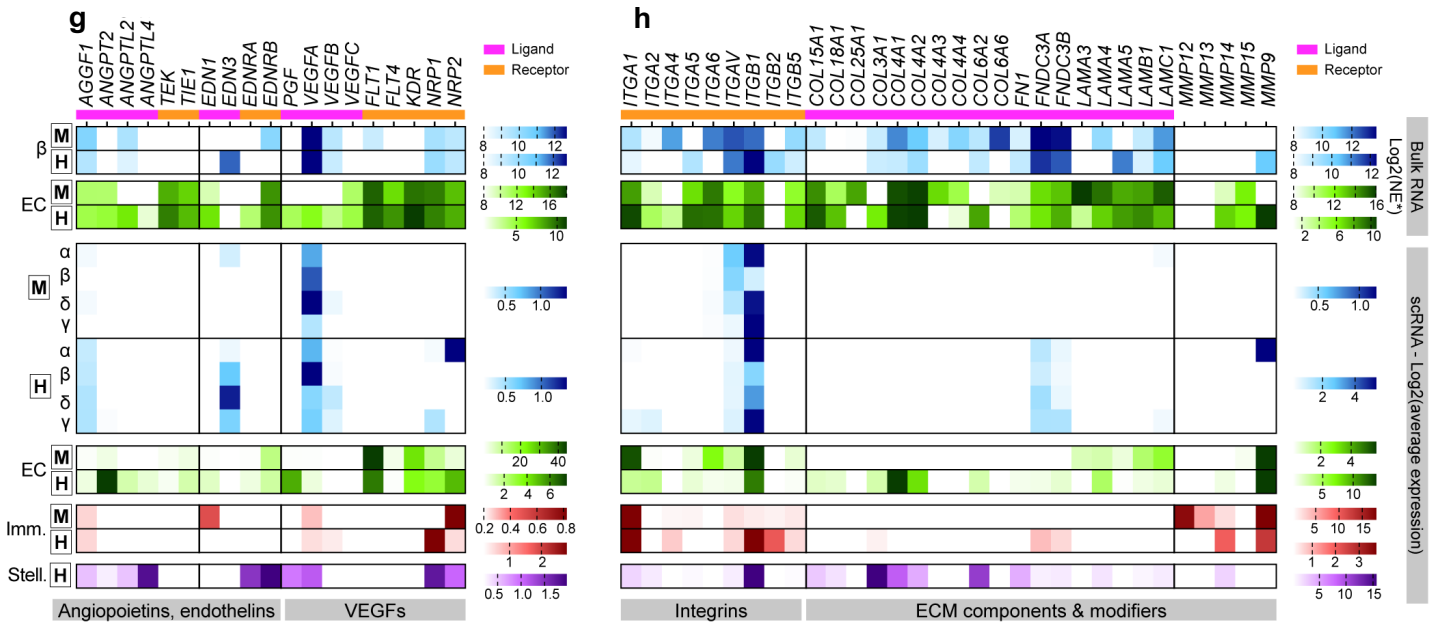

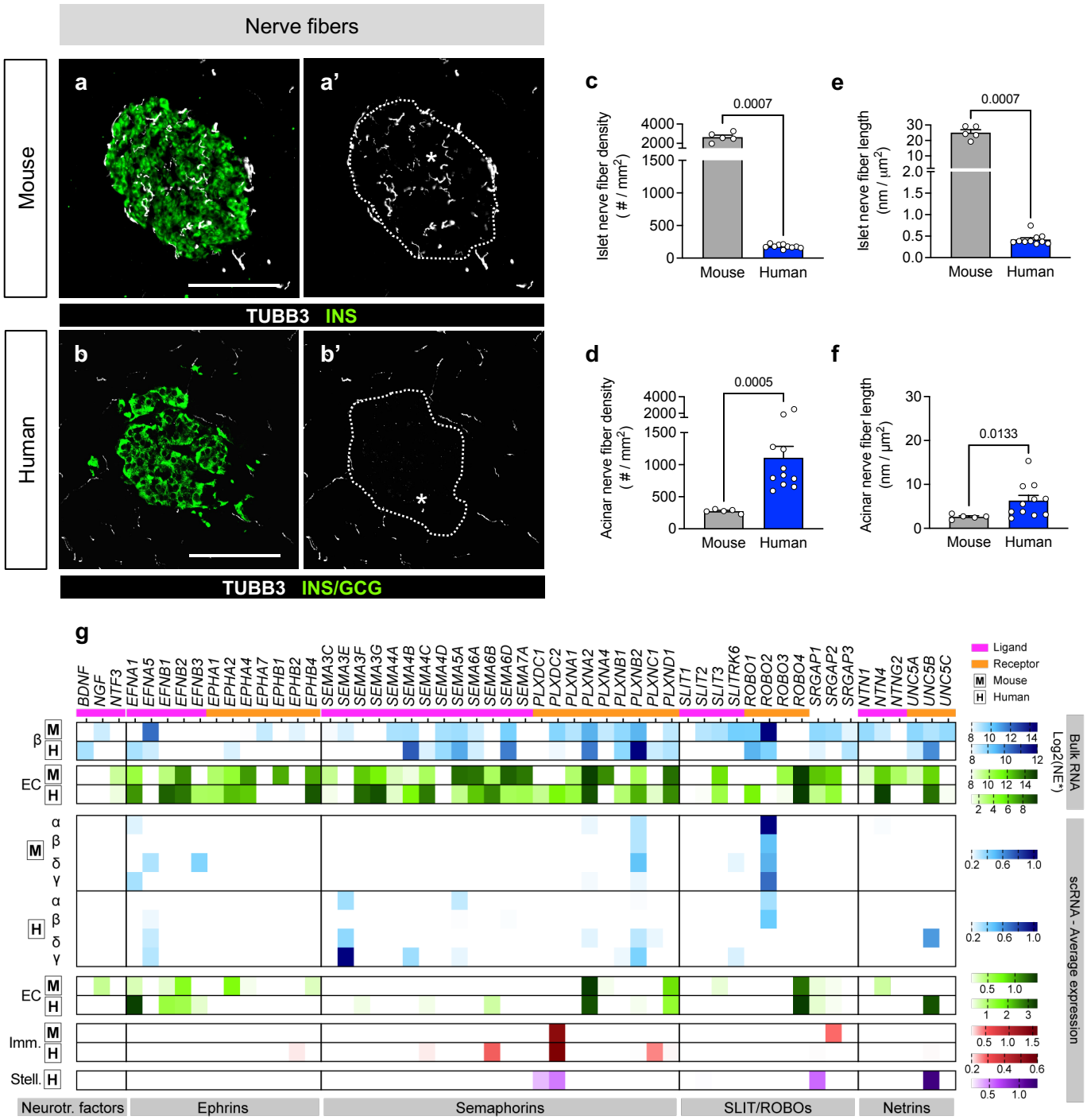

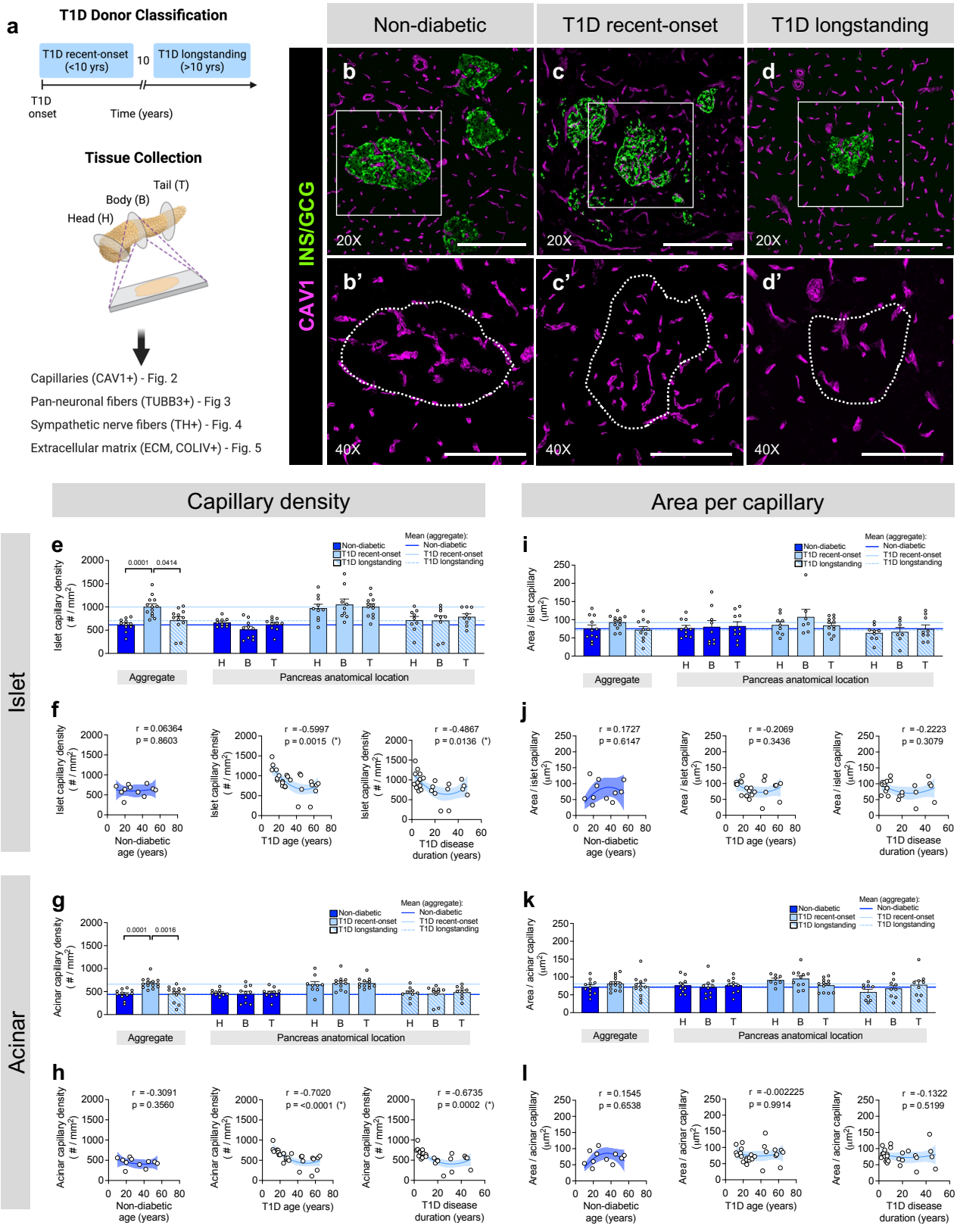

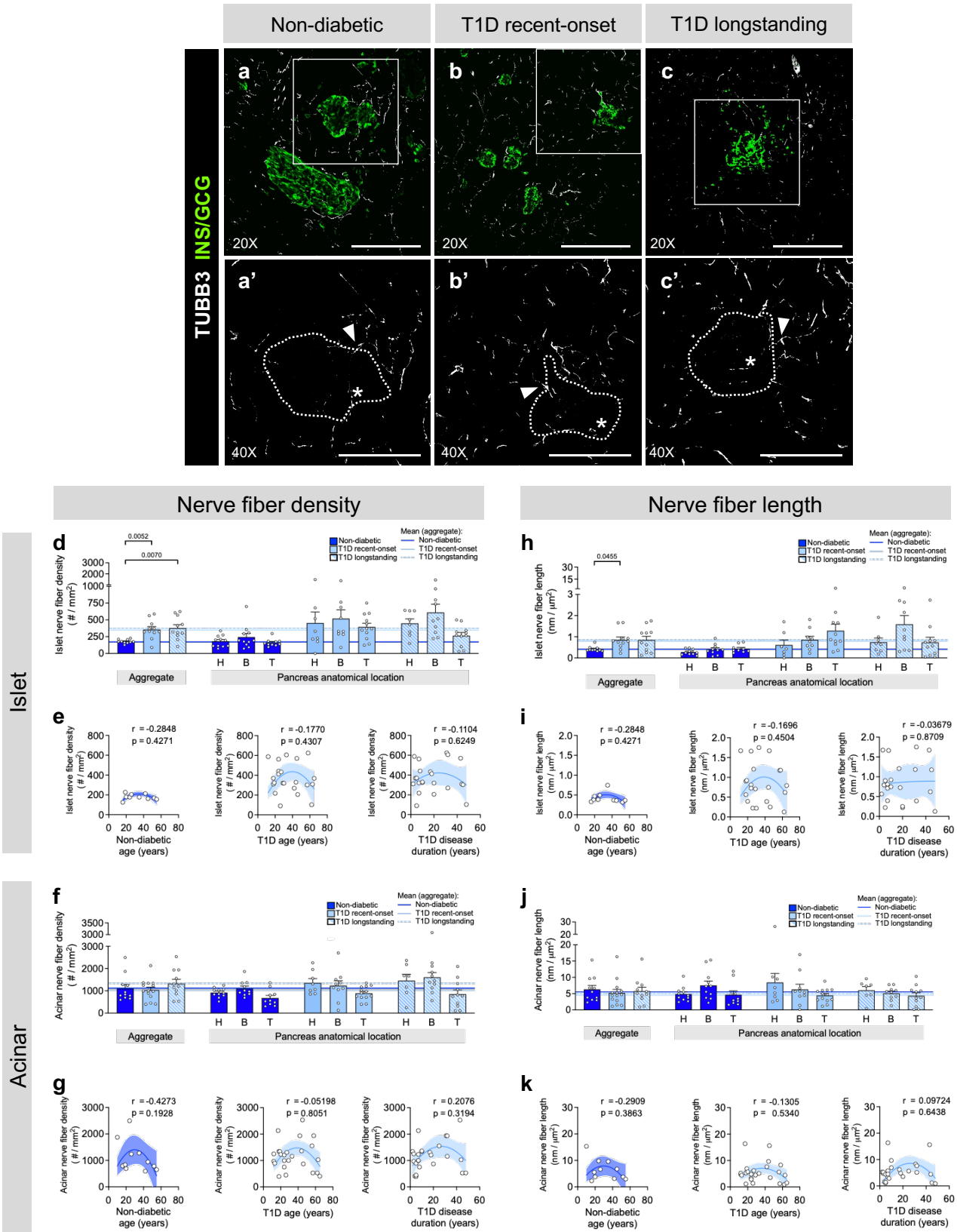

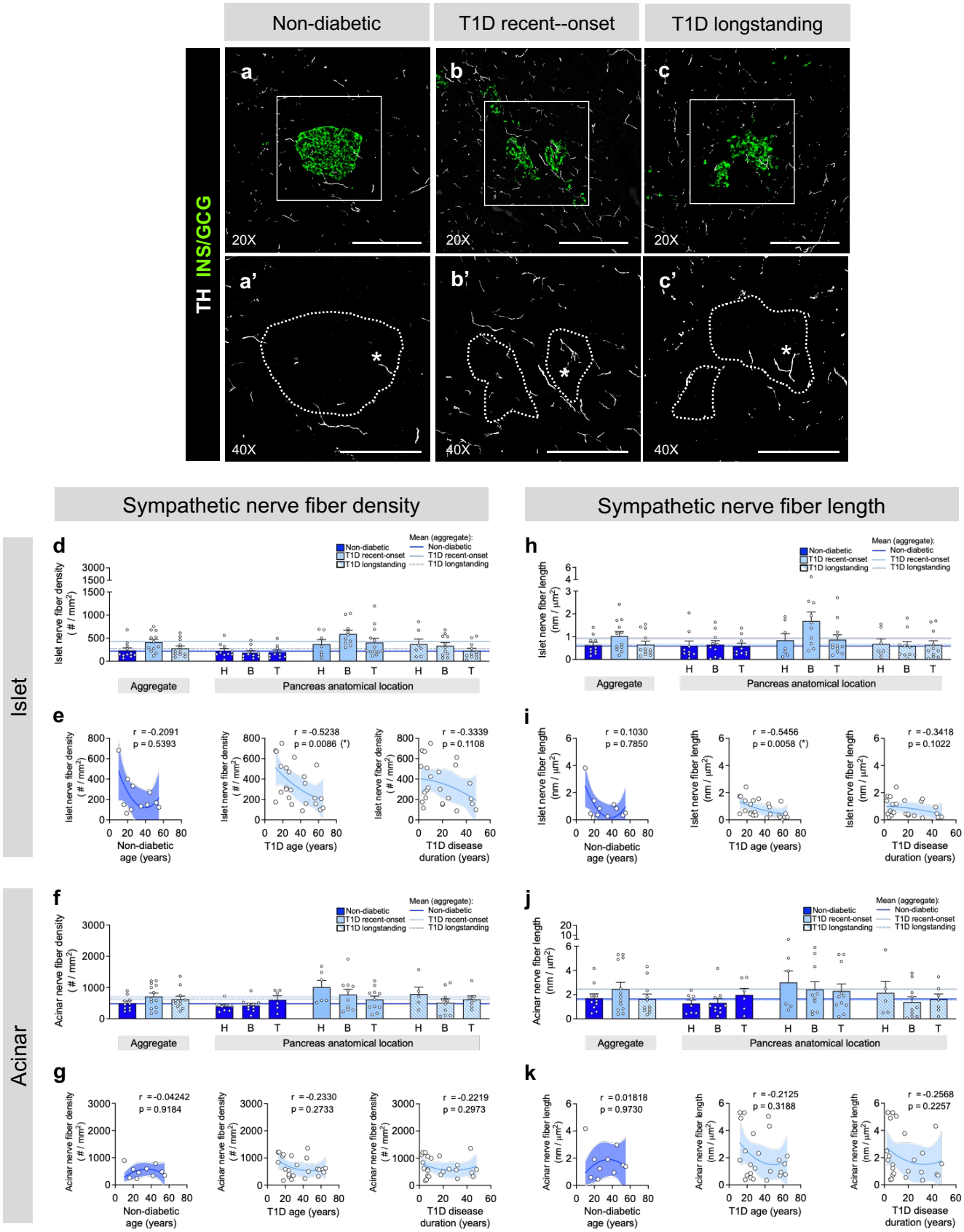

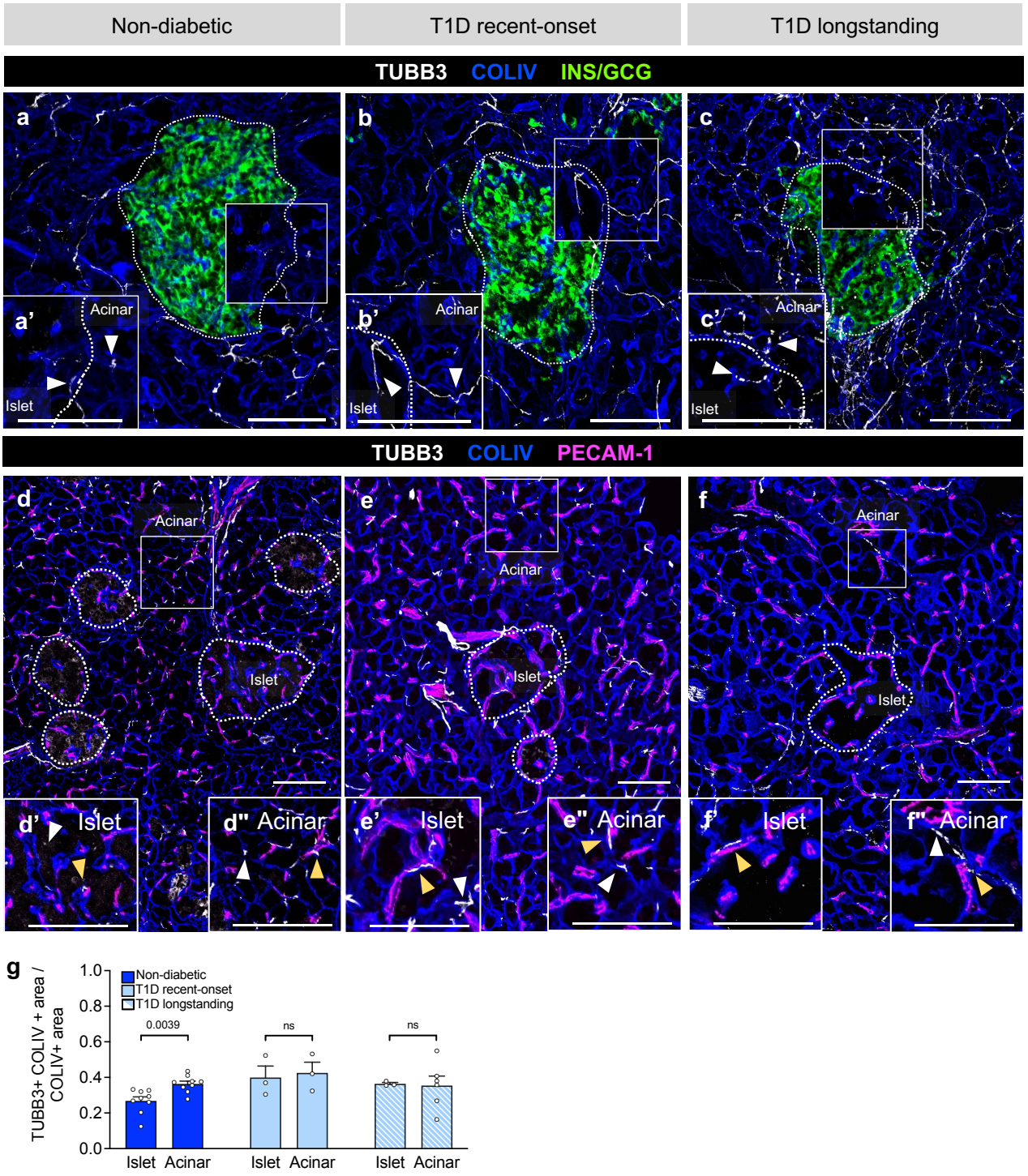

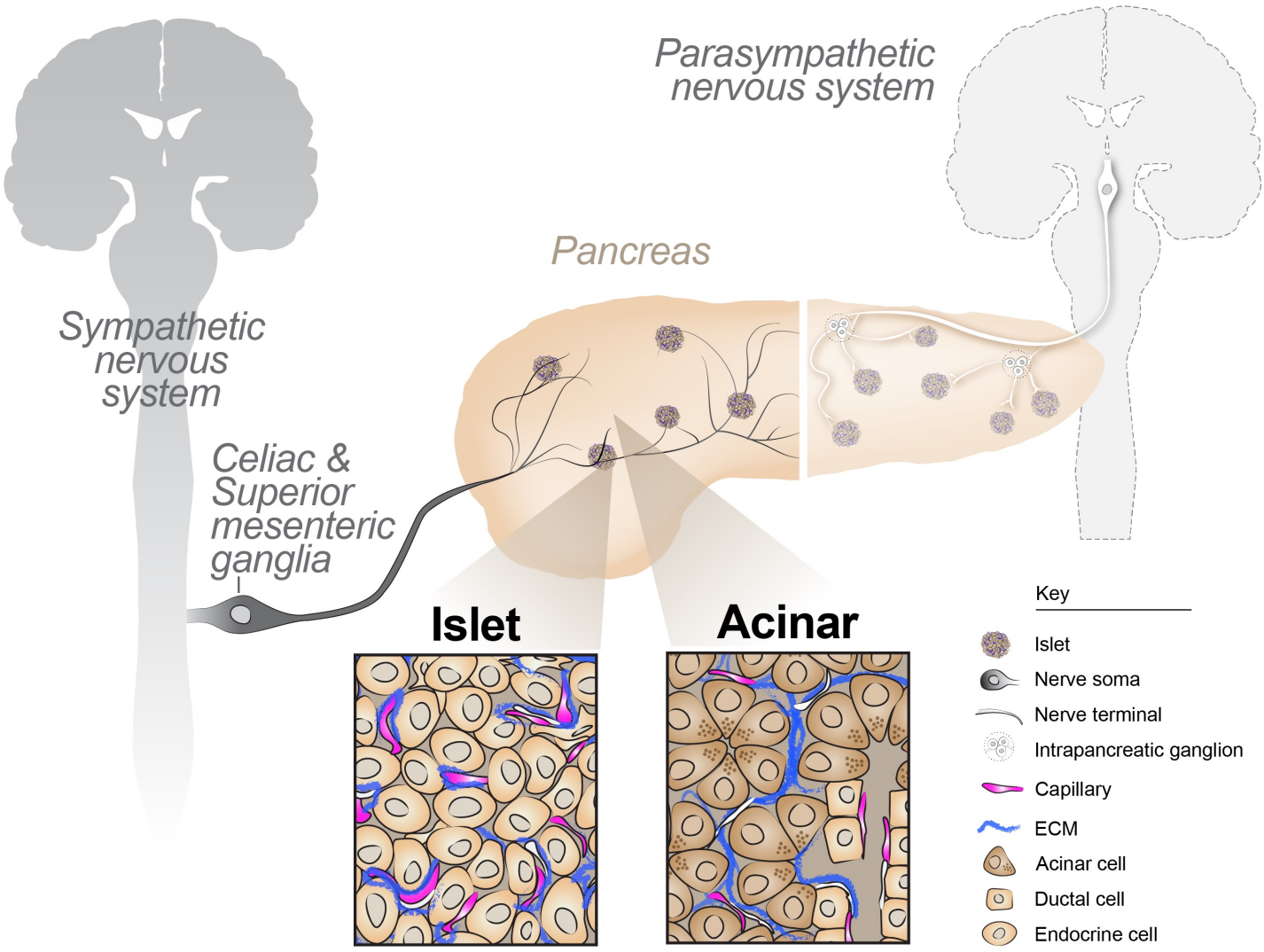

	Capillary density	Nerve fiber density
Inter-species	Mouse > Human (islet & acinar)	Mouse > Human (islet) Mouse < Human (acinar)
Non-diabetic (ND)	ND < T1D recent ND ≈ T1D longstanding	ND < T1D
T1D	T1D recent > ND, T1D longstanding	T1D recent, T1D longstanding > ND
Islet vs. acinar	Islet > acinar (Mouse, ND, & T1D)	Islet > acinar (Mouse) Acinar > islet (Human)

Human pancreatic capillaries and nerve fibers persist in type 1 diabetes despite beta cell loss

METHODS

T1D Donor Classification

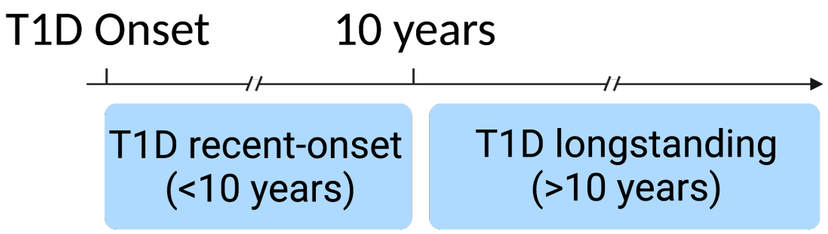

Pancreatic Tissue Sectioning

10 µm and 30 µm section thickness

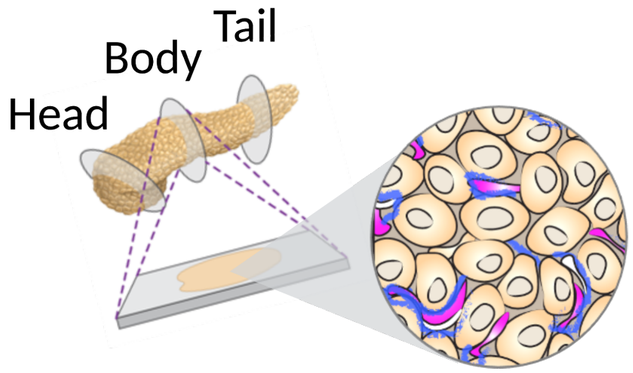

Mutimodal immunofluorescence imaging & morphometric analysis

OUTCOMES

A

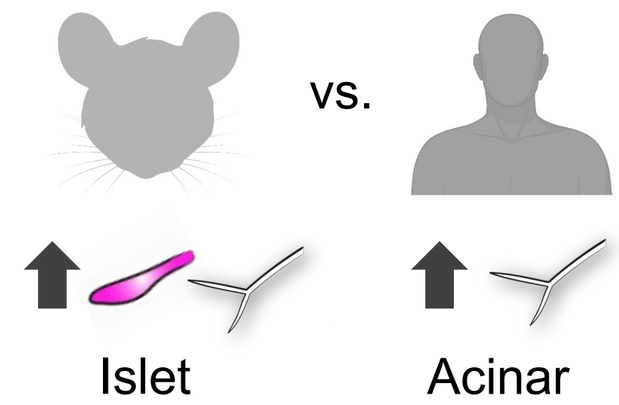

B

All T1D — Islet

- No change detected in sympathetic nerve fiber density

Recent-onset T1D — Islet

C

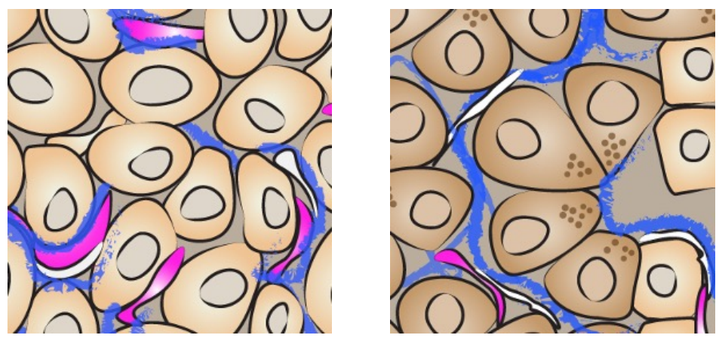

- Fewer nerve fibers associated with capillaries in acinar tissue vs. islets

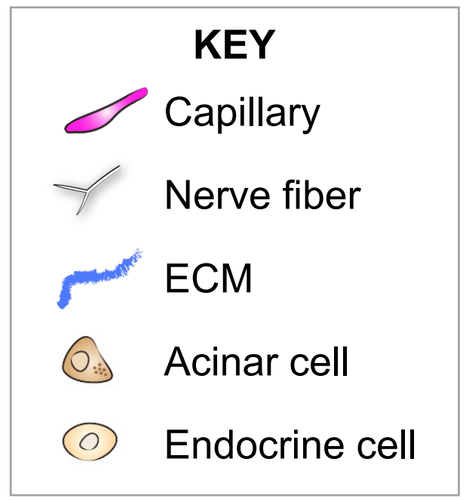

CONCLUSIONS

Pancreatic capillaries and nerve fibers persist in T1D islets and pancreatic acinar tissue despite beta cell loss, suggesting that alpha cell secretory changes may be decoupled from neurovascular components.